NASA Contractor Report 3520

Studies of Single-Mode Injection Lasers and of Quaternary Materials

Volume I - Single-Mode Constricted Double-Heterojunction AlGaAs Diode Lasers

Dan Botez

CONTRACT NAS1-15440
APRIL 1982

NASA

NASA Contractor Report 3520

Studies of Single-Mode Injection Lasers and of Quaternary Materials

Volume I – Single-Mode Constricted Double-Heterojunction AlGaAs Diode Lasers

Dan Botez
RCA Laboratories
Princeton, New Jersey

Prepared for
Langley Research Center
under Contract NAS1-15440

NASA
National Aeronautics
and Space Administration

Scientific and Technical Information Branch

1982

FOREWORD

This program was performed by Boeing Aerospace Company; Kent, Washington for the National Aeronautics and Space Administration, Langley Research Center (NASA LaRC) under NASA Contract 1-14213 from October, 1979 through October, 1980. Mr. John L. Shideler, of the Aerothermal Loads Branch, Loads and Aeroelasticity Division, LaRC, was Technical Monitor for the program.

Boeing Program Manager was Mr. Allan R. Swegle under the administration of Mr. Andrew K. Hepler. Contributors to the program are as follows:

C. H. Bofferding	Test
V. Deriugin	Thermal Analysis
G. A. Dishman	Design
H. Olden	Test
A. R. Swegle	Stress

TABLE OF CONTENTS

LIST OF ILLUSTRATIONS

Figure

LIST OF ILLUSTRATIONS (Continued)

Section

Figure

LIST OF ILLUSTRATIONS (Continued)

Figure

Figure

SUMMARY

Constricted double-heterojunction (CDH) lasers are presented as the class of single-mode nonplanar-substrate devices for which the lasing cavity is on the least resistive electrical path between the contact and the substrate. Various types of CDH structures are discussed while treating three general topics: liquid-phase epitaxy over channeled substrates, lateral mode control, and current control in nonplanar-substrate devices. "Ridge-guide" CDH lasers have positive-index lateral-mode confinement and provide: single-mode cw operation to 7 mW/facet at room temperature and to 3 mW/facet at 150°C; light-current characteristics with second-harmonic distortion as low as -57 dB below the fundamental level; threshold-current temperature coefficients, T_o, as high as 375°C (pulsed) and 310°C (cw); constant external differential quantum efficiency to 100°C; and lasing operation to 170°C cw and 280°C pulsed. "Semi-leaky-guide" CDH lasers have an asymmetric leaky cavity for lateral-mode confinement and provide single-mode operation to 15 to 20 mW/facet cw and to 50 mW/facet at 50% duty cycle. Modulation characteristics and preliminary reliability data are also discussed.

Constricted double-heterojunction diode lasers have demonstrated outstanding cw and pulsed electro-optical characteristics, which make them promising for use in optical communication applications including those cases where single-mode characteristics are desired, such as wavelength multiplexing.

I. INTRODUCTION

The need for mode-stabilized semiconductor diode lasers has generated extensive research efforts (refs. 1-3) in recent years. One successful approach in the quest for stabilization of the lasing mode in the lateral direction (i.e., the plane of the junction) has been one-step crystalline growth over nonplanar substrates (refs. 4-18). The vast majority of nonplanar-substrate structures relies on the growth characteristics of liquid-phase epitaxy over channels etched into the substrate (refs. 5,6,19,20). The results have been mode-stabilized devices of remarkable characteristics: single-mode cw operation to relatively high powers (20 to 40 mW/facet) (refs. 8,14); relatively low threshold currents (12 to 30 mA) (refs. 13,15,18,21,22); highly linear light-current curves (ref. 12); and for some geometries (refs. 18,23,24) exceptionally low threshold-current temperature dependence in both pulsed (T_o = 240 to 375°C) and cw (T_o = 200 to 310°C) operation (ref. 23). In this report we present and discuss one family of nonplanar-substrate devices: constricted double-heterojunction (CDH) diode lasers. The two types of practical CDH devices are shown in Figure 1: ridge guide and semileaky guide. For both types lateral mode control is achieved via active-layer-thickness variations "built in" during LPE growth above the mesa separating two adjacent channels. The optical cavity is thus on the shortest distance from the contact to the substrate and for that reason such structures are called constricted. As discussed below, the constricted geometry provides not only lateral optical mode control but lateral current control as well and, under certain conditions, is directly responsible for a low threshold-current temperature sensitivity. In order to understand what factors led to the development of CDH devices and how CDH devices differ from other nonplanar-substrate lasers, we start by treating three topics directly related to nonplanar-substrate-laser behavior: growth characteristics of LPE over nonplanar substrates, lateral mode control, and current control. Then, for two types of CDH lasers (fig. 1), we describe and discuss in detail fabrication procedures, lateral mode control, and electro-optical (cw and pulsed) characteristics relevant to optical communications applications. Emphasis is placed on ridge-guide devices, since this is the first complete description of their operational characteristics.

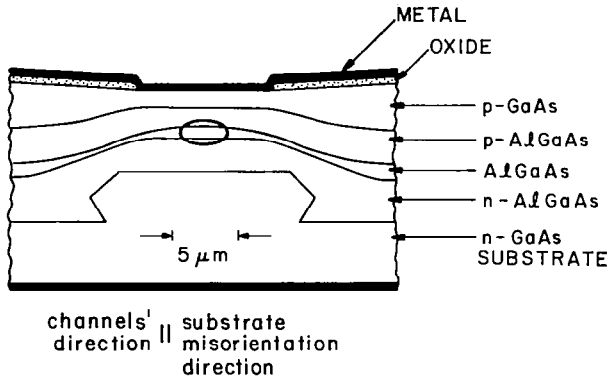

(a)

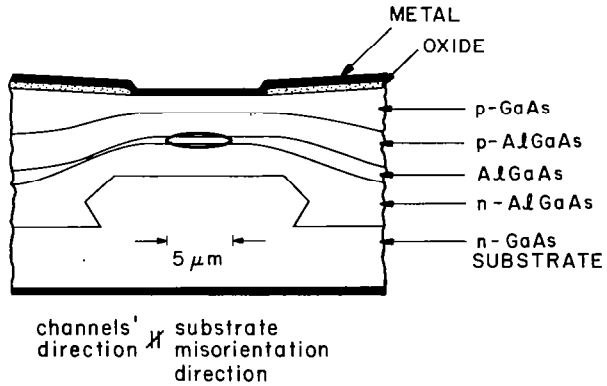

(b)

Figure 1. Schematic representation of the two practical types of constricted double-heterojunction lasers: (a) the ridge-guide type and (b) the semileaky-guide type. Either type can be obtained by controlling the relative position of the channels' direction with respect to the substrate misorientation direction. See text.

II. GENERAL CONSIDERATIONS

A. LIQUID-PHASE EPITAXY OVER NONPLANAR SUBSTRATES

The discovery of the fact that LPE growth is strongly affected by topographical features etched into the substrate (channels, terraces, mesas) occurred independently in 1975 at three laboratories (refs. 4-6). The first nonplanar-substrate laser was reported by Burnham and Scifres (ref. 4). Studies of LPE growth characteristics over channels have been done by Botez et al. (refs. 5,25), Kirkby and Thompson (ref. 6), Funakoshi et al. (ref. 19), and Andreev et al. (ref. 20). To illustrate these characteristics we show schematically in Figure 2 the growth stages above a channel (fig. 2a), a terrace (fig. 2b), and a mesa (fig. 2c). Before going any further it must be stressed that in all cases considered here the material used as mask for substrate etching is removed prior to growth, and thus growth over substrate channels defined by oxide films (refs. 20,26) will not be treated.

The substrates are in all cases (100) oriented. The various substrate-surface features are obtained by preferential chemical etching through windows in oxide masks. The main driving force for nucleation is the LPE-growth dependence on local surface curvature. It can be shown from thermodynamic considerations (ref. 27) that for a given temperature, variations in surface curvature are associated with variations in chemical potential of the solid. In order to maintain equilibrium, variations in chemical potential of the solid have to be matched by variations in chemical potential of the liquid solution, which in turn are directly related to relative deviations in solute concentrations, C (i.e., $\Delta\mu = kT\ \Delta C/C$). Then one obtains, for equilibrium near a curved solid surface of radius R, the following relationship (refs. 25,27):

$$\frac{\Delta C}{C} = \frac{2\gamma\ V_m}{kT}\ \frac{1}{R} \tag{1}$$

where γ is the surface tension, V_m is the crystal molar volume, and R can be positive or negative depending on whether the surface is convex or concave, respectively. As shown in Figure 3, the net effect is that at a fixed temperature, T_e, for which equilibrium exists between a solution of solute concentration C_e and a planar surface, the curved surfaces will be in equilibrium for different solute concentrations: $C_e \pm \Delta C$ depending on whether the surface is convex or concave. Conversely, at a given solute concentration C_e, equilibrium

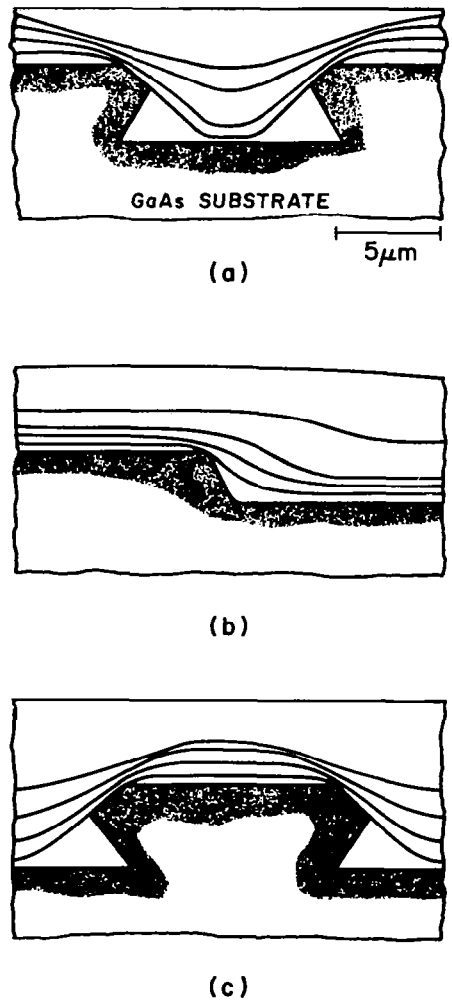

Figure 2. Schematic representation of liquid-phase-epitaxial growth stages over various topographical features etched into GaAs substrates: (a) a channel, (b) a terrace, and (c) a mesa.

will be reached at the temperatures $T_e \pm \Delta T$ for concave and convex surfaces, respectively. Thus, a melt of concentration C_e at T_e is: (1) effectively undersaturated for the convex case with subsequent melt-etch of the convex surface and (2) effectively supersaturated for the concave case with subsequent rapid growth on the concave surface. As can be seen from Figure 2, there is always a tendency to fill in concave parts of the surface (e.g., bottom corners of dovetail-shaped channels) and melt-etch convex parts of the surface (e.g., channel "shoulders"). The preference of LPE growth for concave over convex

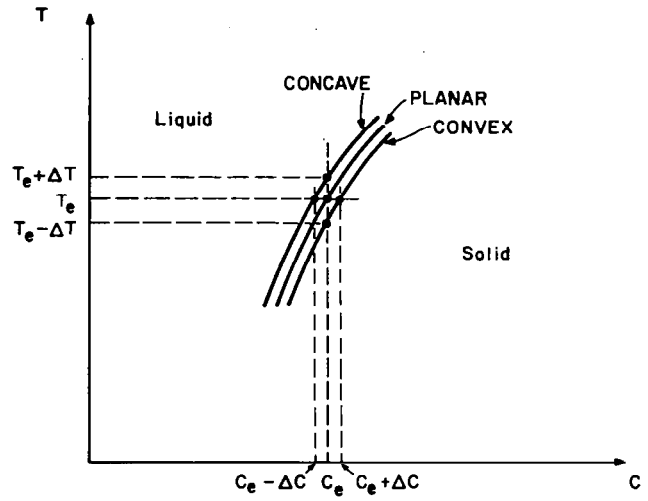

Figure 3. Liquidus curves for planar, concave, and convex surfaces around temperature T_e. At T_e a solid of planar surface is in equilibrium with a liquid of solute concentration C_e.

surfaces, while most evident in the incipient growth stages over channels, is still a major factor in the shaping of the various grown layers (refs. 5,6,25). Another important factor is lateral mass transfer from melt-etched areas (e.g., channel shoulder) or planar areas (e.g., flat bottoms for channels) to concave areas. Then the driving forces are on one hand differences in surface tension along the liquid-solid interface (refs. 5,25) as the curvature varies, and on the other hand lateral diffusion induced by local solute concentration gradients between melt-etched areas and filled areas (ref. 19). The overall tendencies are rapid growth in concave areas and slowed growth in convex areas so that the total surface free energy is minimized with the eventual result of obtaining a flat surface.

The various growth stages over a channel, a terrace, and a mesa are illustrated in Figure 2. Just as discussed above, in all cases growth occurs preferentially in concave areas over convex areas with the tendency to eventually flatten the surface. Depending on the structure geometry that one seeks to obtain, one can control the growth features not only by such obvious parameters as etched-channel geometry, but also by growth conditions such as the amount of supercooling (refs. 5,19), the growth temperature (refs. 5,19), and

the cooling rate. For instance, melt-etch of the channel shoulders can be prevented by using initial supercooling (2 to 10°C) (refs. 5,19), relatively low growth temperatures (700 to 780°C) (refs. 5,19), and fast growth rates (1 to 2°C/min) (refs. 5,19). Another growth characteristic, fast fill-in of channel to a flat surface (as needed in channel-substrate-planar structures), also requires low growth temperatures (ref. 5), but moderate supercooling and growth rates (ref. 19). In all of the above cases, the substrate is considered to be oriented perfectly in the (100) direction. However, if the substrate is misoriented with respect to the (100) direction, growth over channels can be dramatically affected, as discussed in Section III.

B. LATERAL OPTICAL MODE CONTROL IN NONPLANAR-SUBSTRATE DEVICES

Growth over topographical features in a substrate will provide lateral mode control via (1) lateral variations in layer thickness in and around the lasing region and (2) the presence of a high-index, highly absorbing substrate in close proximity to the lasing region. Some of the structures that have thus emerged are displayed later in Figure 5. Variations in active-layer thickness can be directly translated into lateral variations of the effective refractive index, N_{eff}, as shown in Figure 4. The basic formula for N_{eff} is (refs. 28,29):

$$N_{eff}(x) = \sqrt{n_2^2 + F(x)\,(n_1^2 - n_2^2)} \qquad (2)$$

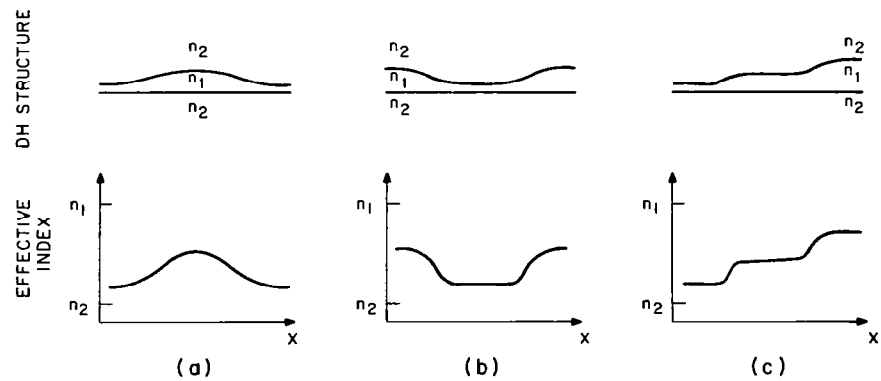

Figure 4. Types of wave-confining structures which result from variations in active-layer thickness: (a) positive-index guide or ridge guide; (b) negative-index guide or leaky guide; and (c) ladder-index guide or semileaky guide.

where n_1 and n_2 are the active and cladding-layers bulk refractive indices, respectively, x is displacement in the lateral direction, and F is an active-layer filling factor related to the electromagnetic field. For structures of varying active-layer thickness F corresponds to b, the field amplitude filling factor (refs. 28,30), which to first order is approximated by Γ, the field intensity (power) filling factor (ref. 31). By using accurate analytical approximations (refs. 32,33), we transform equation (2) into

$$N_{eff}(x) \cong n_2 + \frac{D^2(x)}{2 + D^2(x)} (n_1 - n_2) \tag{3}$$

with $D(x) = \frac{2\pi}{\lambda} d(x) \sqrt{n_1^2 - n_2^2}$

where d(x) is the active layer thickness as a function of position and is the vacuum wavelength. From equation (3) it is clear that the relative variation of the effective index (i.e., $N_{eff} - n_2$) increases with increasing active-layer thickness. For relatively small active-layer thicknesses ($d < 0.15$ μm) the relative index variation is almost proportional to d^2. We show in Figure 4 three types of wave-confining structures, according to the lateral variation in N_{eff}: (a) "positive-index" waveguide or ridge guide, for which N_{eff} has a local enhancement; (b) "negative-index" waveguide or leaky guide for which N_{eff} has a local depression; and (c) "ladder-index" waveguide or semileaky guide, which is guiding to one side and "antiguiding" to the other side. A positive-index guide can be designed (width, maximum thickness, degree of tapering) (refs. 6,15,34) to support only the fundamental optical mode; that is basically the only lateral mode selection mechanism at lasing threshold. By contrast, in negative- and ladder-index waveguides the mode selection relies on mode-dependent lateral radiation losses. For instance, a negative-index guide of width w_o and net index depression Δn has lateral radiation losses (refs. 35,36):

$$\alpha_R \cong \frac{m^2 \lambda^2}{2 w_o^3 n_o^2 \sqrt{2 \Delta n / n_o}} \tag{4}$$

where m is the mode number and n_o is the index of refraction in the outer regions. The losses for the first-order mode (m = 2) are four times the losses for the fundamental mode (m = 1). In a passive dielectric waveguide these leaky modes could not be supported for long distances due to their radiation

losses. However, in an active leaky-guide structure, electronic gain can overcome the radiation losses and allow sustained propagation and oscillation of leaky modes. Then the mode-dependent losses assure lasing to relatively high powers in the single-mode regime.

Structures for which lateral mode control can be attained by variations in active-layer thickness alone are the channeled-substrate narrow stripe (CNS) laser (ref. 21 and fig. 5a), the leaky-guide CDH laser (ref. 9 and fig. 5c), the terraced-substrate (TS) laser (ref. 11 and fig. 5d), the ridge-guide CDH laser (ref. 18 and fig. 5e), and the semileaky guide CDH laser (ref. 10 and fig. 5f). Of these, the CNS, TS, and ridge-guide lasers have positive-index lateral mode confinement (fig. 4a), the leaky-guide CDH laser has negative-index confinement (fig. 4b), and the semileaky-guide CDH laser has ladder-index confinement (fig. 4c). Displayed in Figure 6 are the main types of lateral waveguides for low-threshold cw CDH lasers. The active-layer thickness variations are drawn to scale from actual structures (for display purposes the vertical scale is ten times larger than the horizontal scale). The ridge-guide structure provides, as expected, a bell-shaped effective-index lateral variation. Due to its lens-like shape, in the ridge guide the propagating light is focused to a relatively small spot (refs. 6,15) (i.e., 1.5 to 2.5 μm at $1/e^2$ points in intensity for 3- to 6-μm wide guides). A large spot size is generally desired since that assures higher power capabilities (ref. 31). Increases in spot size can be achieved either by allowing for extremely mild lateral thickness variations or by growing an additional propagating layer (i.e., large optical cavity) of the negative-index type (ref. 14).

The semileaky type devices provide a ladder-index lateral profile. To one side the light is totally reflected just as in a ridge-guide, while to the other side light is only partially reflected with the transmitted part acting as radiation loss, α_R. For a typical case (i.e., w_o = 5 to 6 μm and Δn = 0.02) it is found that α_R has reasonable values (12 to 20 cm^{-1}) when compared to the mirror losses. Due to the defocusing effect on the leaky side, the semileaky guide supports wider laser spots (3.5 to 6 μm) than ridge guides of comparable lateral extent. As will be shown in Section V, semileaky-guide structures by their leaky nature also allow single-mode operation to higher powers than the ridge-guide structures, but at a price in threshold current and temperature sensitivity of the threshold. Other features of leaky-guide devices such as sidelobes in the far-field pattern are presented in Section V.

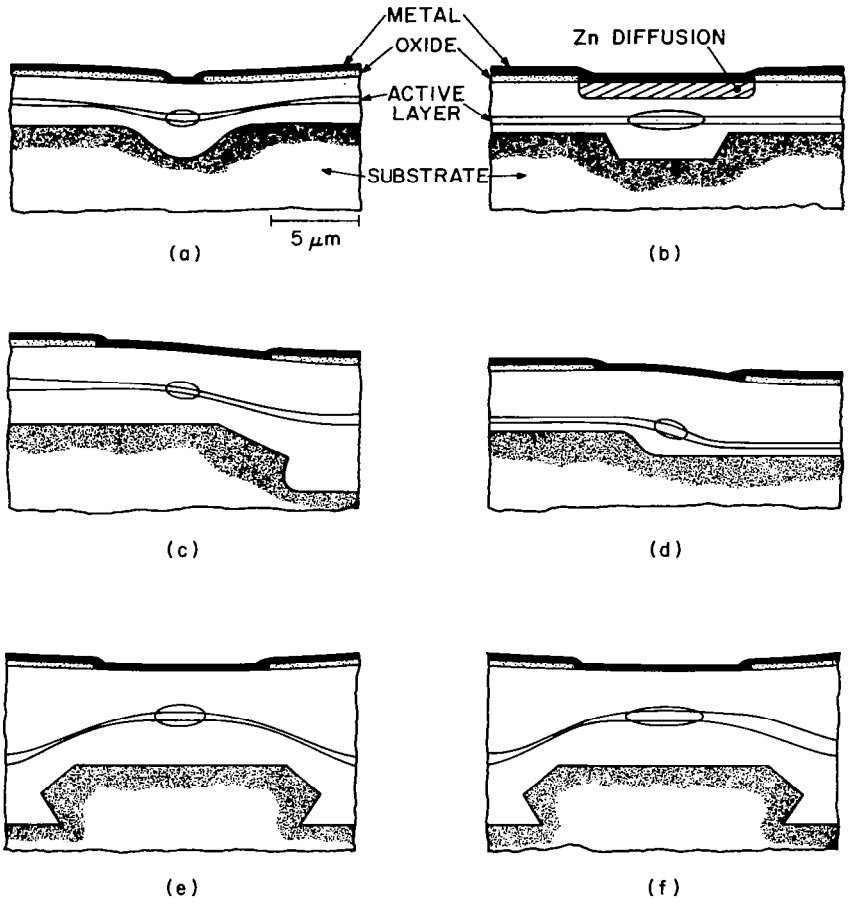

Figure 5. Types of nonplanar-substrate mode-stabilized devices: (a) the channeled-substrate narrow-stripe (CNS) laser (ref. 21); (b) the channeled-substrate-planar (CSP) laser (ref. 8); (c) the leaky-guide constricted double-heterojunction (CDH) laser (ref. 9); (d) the terraced-substrate (TS) laser (ref. 11); (e) the ridge-guide CDH laser (ref. 18); and (f) the semileaky-guide CDH laser (ref. 10).

As mentioned above, the other factor which can determine lateral mode control is the proximity of a highly absorbing high-index substrate. Best use of such an effect has been made for CSP devices (ref. 8 and fig. 5b). It can be shown (ref. 37) by solving the wave equation that in the region above the channel N_{eff} is larger than in the regions away from the channel. Thus, a positive-index waveguide is created. More recent analyses (ref. 38) show that

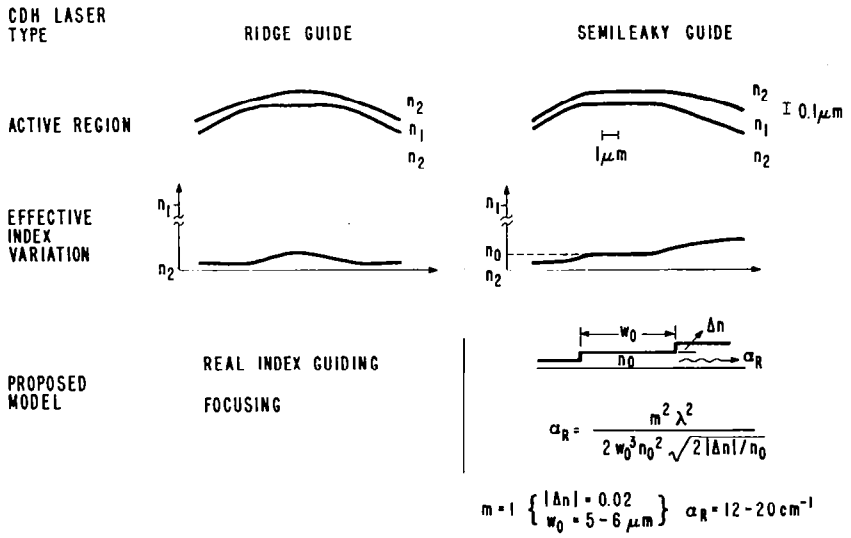

Figure 6. Diagram of typical active-layer thickness variations for ridge-guide and semileaky-guide devices, the respective variations in effective refractive index, and the respective mode confinement and selection mechanisms. The loss coefficient α_R is radiative loss in the semileaky guide, and m is the mode number (see text).

antiguiding is also present. Discrimination against high-order lateral modes is caused by lateral absorption and/or radiation losses to the substrate. Similar mode discrimination has been realized for CNS structures (ref. 39) by growing relatively thin n-AlGaAs material above the shoulders of a narrow channel.

In all nonplanar-substrate structures shown in Figure 5 it is assumed that the current flow is uniform across the lasing area. This, however, is not true for structures where the lasing cavity lies above a channel (e.g., CNS and CSP) unless steps are taken during the fabrication to tightly confine the current to the lasing cavity (refs. 7,8,21). The next subsection treats this subject.

C. CURRENT CONFINEMENT IN NONPLANAR-SUBSTRATE DEVICES

Unlike stripe-contact lasers, in nonplanar-substrate devices the size of the lasing mode in the lateral direction is solely determined by "built-in"

real-index lateral waveguides or antiwaveguides (see fig. 5). However, if the current flow is highly nonuniform across these lasing cavities, high-order modes may be preferred to operate over the fundamental one (ref. 3). We illustrate in Figures 7a and b how currents tend to flow in nonplanar-substrate structures without lateral current confinement. In both cases we have topographical features in a highly conductive substrate over which highly resistive AlGaAs layers are grown. Given a flat top surface on which a "standard"-width (10 to 12 μm) contact stripe is placed, the current will seek the least resistive paths. For a nonplanar-substrate structure grown over a channel, the least resistive paths are from the stripe contact at the channel shoulders. Furthermore, as current is increased, lateral voltage differentials due to parallel current paths of different resistance will cause the current(s) to "crowd" toward the channel shoulders. Such current "filamentation" effects are well known in power transistors. A structure particularly prone to nonuniform current flow is the CSP structure (fig. 5b) without preferential Zn diffusion, since in that structure the moderately resistive n-AlGaAs layer is 4 to 7 times thicker above the channel than away from the channel. Then the current flows mostly toward the channel shoulders (ref. 3 and see fig. 7a) causing the electronic gain distribution to be peaked in those regions, and thus favoring lasing of high-order modes. For that reason, in CSP devices a relatively uniform current flow across the channel is assured by a deep Zn diffusion 2 to 3 μm wider than the channel (ref. 8 and see fig. 5b). Other tight-current-confinement techniques for nonplanar-substrate structures with the lasing cavity above a channel are very narrow oxide-defined stripes (2 to 4 μm) (refs. 12,21), narrow stripes defined by proton bombardment (ref. 22) or back-biased junctions (ref. 13), and current-blocking layers (refs. 3,7,15) in the planar areas away from the channel. Figueroa (ref. 40) has shown that depending on the degree of current blockage by back-biased junctions, the current can either crowd toward the channel shoulders (i.e., poor current blockage) or concentrate above the channel (i.e., good current blockage).

The situation is quite different when the structure is grown over a highly conductive substrate mesa (fig. 7b). When the stripe contact is placed above the mesa, the current flows uniformly toward the mesa as that is the least resistive electrical path between contact and substrate. The very shape of the

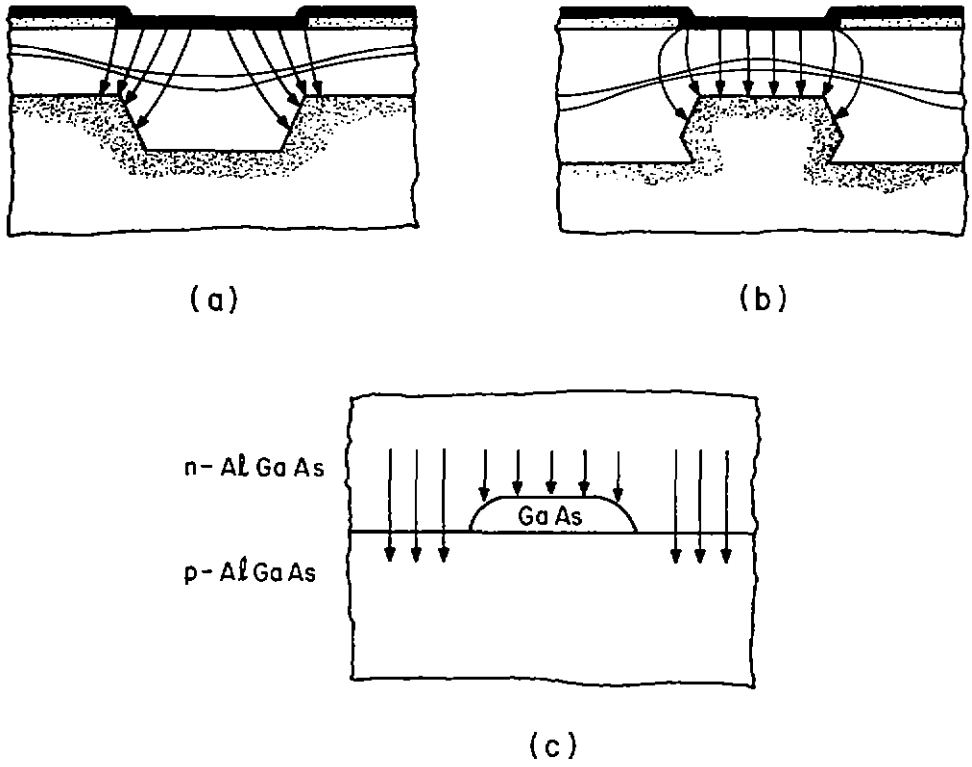

Figure 7. Schematic diagrams of current flow in: (a) AlGaAs structure grown over a channel of highly conductive GaAs substrate; (b) AlGaAs structure grown over a mesa of a highly conductive GaAs substrate; (c) AlGaAs structure with discontinuous active layer. In (c) the currents outside the active layer are resistive-shunt currents.

highly resistive p-AlGaAs layers (i.e., of minimum thickness above the mesa and tapering sideways to larger thicknesses) favors concentration of the current toward the mesa. As discussed in Section IV.C a current crowding effect toward the mesa is responsible for an unusually low threshold-current temperature dependence in ridge-guide CDH lasers. In those cases the current does not have to be confined to narrow stripes for lasing to occur in the fundamental mode. The absence of a requirement for special current-confining techniques makes CDH structures easier to fabricate than other nonplanar-substrate structures.

Structures grown over channel shoulders (fig. 5c) or over terraces in the substrate (fig. 5d) can have significant current-flow problems. Depending on

the structure geometry and the position of the stripe contact, such structures may or may not lase in the intended cavity (refs. 9,11,34). For instance, in TS devices (ref. 11) unwanted lasing in the region closest to the terrace shoulder is prevented by growing the structure such that the active layer in the planar area is very close (0.3 to 0.4 μm) to the highly absorbing substrate. In general, structures grown over substrate mesas (i.e., the practical types of CDH lasers depicted in fig. 1, and the mesa-substrate buried heterostructure laser, ref. 16) are the only ones for which the current flow does not interfere with the excitation of the fundamental mode.

Another issue related to current flow in nonplanar-substrate structures is resistive-shunt leakage through areas without active layers (fig. 7c). Such areas can be obtained by design due to melt-etch on convex parts of the n-AlGaAs layer (refs. 4-6) or lack of growth on the (111)A planes of InP-based structures (ref. 16). An isolated active region is then obtained which, due to large lateral index differential, has to be relatively narrow (2 to 4 μm, ref. 15) to support only the fundamental mode. Such structures have been realized (refs. 4,6,16) but with generally high pulsed thresholds and poor cw operational characteristics. The reason is that although the saturation current density of a p-n AlGaAs junction is several orders of magnitude lower than the saturation current density of a p-n GaAs-AlGaAs junction, at the current densities needed in lasing (i.e., 1 to 3 kA/cm^2), the current densities passing through either type of junction are comparable (ref. 41). This is due to the series resistance of the diode laser, as shown by Tsukada et al. (ref. 41). The resistive-shunt currents on either side of the active region not only increase the overall current but also create heating which may severely affect cw operation. A good example of a structure with severe resistive-shunt currents is the original strip buried-heterostructure (SBH) laser (ref. 42) which, while providing high powers in low-duty cycle (10^{-4}) operation, could not be made to lase either at thresholds below 100 mA and/or cw unless the current was tightly confined to the active-layer strip by back-biased junctions or proton bombardment (ref. 43). For the reasons stated above, all nonplanar-substrate structures of cw operational capability (fig. 5) have active layers that are contiguous across the device area.

III. FABRICATION PROCEDURES

The fabrication steps for CDH devices are schematically shown in Figure 8. The first step is the etching of the channels. The GaAs substrates chosen for this are Si doped (2 to 3×10^{18} cm^{-3}) and of a controlled degree of misorientation, α, with respect to the (100) plane. As shown in Figure 9, the degree of misorientation α is defined with respect to a specific crystallographic direction [hkl]. In our case the substrate misorientation direction was chosen to be either parallel to the channels' direction (i.e., [011]) or at 45° with respect to the channels' direction (i.e., along [010]). A typical example is a substrate misoriented 1° off the (100) plane and toward the [011] direction. As discussed below and illustrated in Figure 9, the substrate misorientation plays an important role in determining the shape of the lasing cavity.

The channels used have invariably been dovetail-shaped; that is, parallel to the [011] direction on a (100)-oriented GaAs substrate. The reason V-shaped channels are not used is that during LPE growth, the mesa separating a pair of V-channels can be easily melt-etched, which in turn prevents the formation of a convex surface above the mesa, the very characteristic of the CDH geometry. By contrast, the mesa between two dovetail channels is melt-etched only at the sharp convex shoulders of those channels (see fig. 8), and thus grown layers of negative curvature can easily be attained above the mesa (bottom of fig. 8). The channels' etching is performed by using SiO_2 window masks and the solution 1:8:8 (H_2SO_4:H_2O_2:H_2O) at 20°C. Pairs of 5-μm-wide stripes are originally formed in SiO_2 with the help of standard photoresist techniques. Then the etchant is used for ∿1 minute to form 4-μm-deep channels of 10-μm-wide top widths. The interchannel spacing can take values between 24 and 40 μm with a typical value of 32 μm. The SiO_2 film is subsequently removed with buffered HF, and the whole surface is lightly etched with a NaOH:H_2O_2 aqueous solution (8 gm Na OH in 200 ml water and 20 ml H_2O_2 (30%) in 200 ml water) for 1 minute. The channeled substrate is then cleaned and loaded into the LPE boat.

Liquid-phase epitaxy is performed by the thin-solution technique (ref. 44) which allows reproducibility and uniformity in the deposition of thin layers (<0.2 μm). Growth of at least four epitaxial layers occurs between 850 and 820°C while the cooling rate is ∿1°C/min. Thus, as opposed to CSP structures

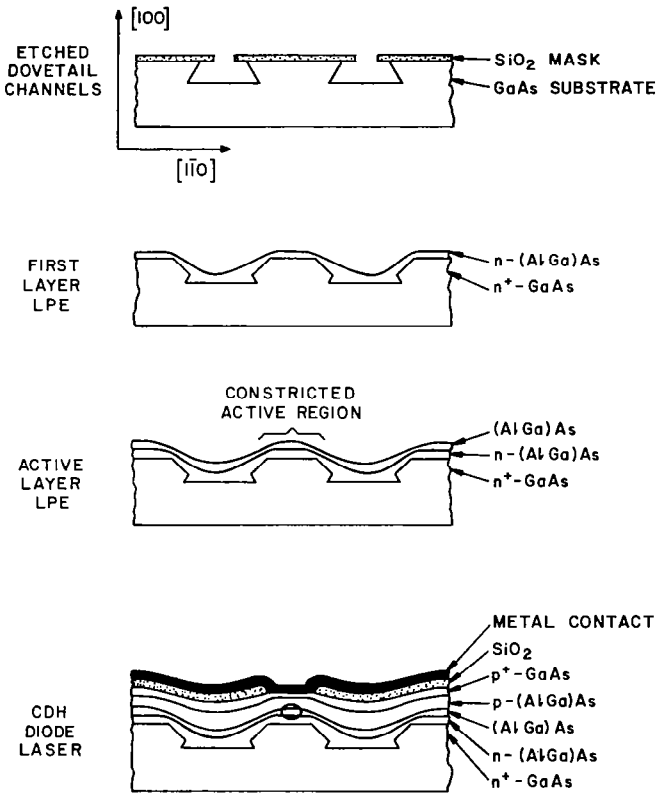

Figure 8. Schematic representation of the fabrication steps of CDH devices. A ridge-guide device is considered.

(ref. 19), the growth temperatures for CDH devices are not limited to values below 780°C. During the first-layer growth (i.e., n-AlGaAs) the channel shoulders are partially and preferentially melt-etched (fig. 8). In order to avoid heavy melt-etch, a controlled amount of cooling (3 to 5°C) is provided before the introduction of the substrate under the first solution. The active layer is subsequently grown. Its lateral thickness variation is dictated both by local surface curvature as well as by the relative position of the channels' direction with respect to the substrate misorientation direction (see fig. 11). After growth of a four-layer CDH structure, standard oxide-stripe technology is used for placing 10-μm-wide metallic stripe contacts above the mesa separating the channels.

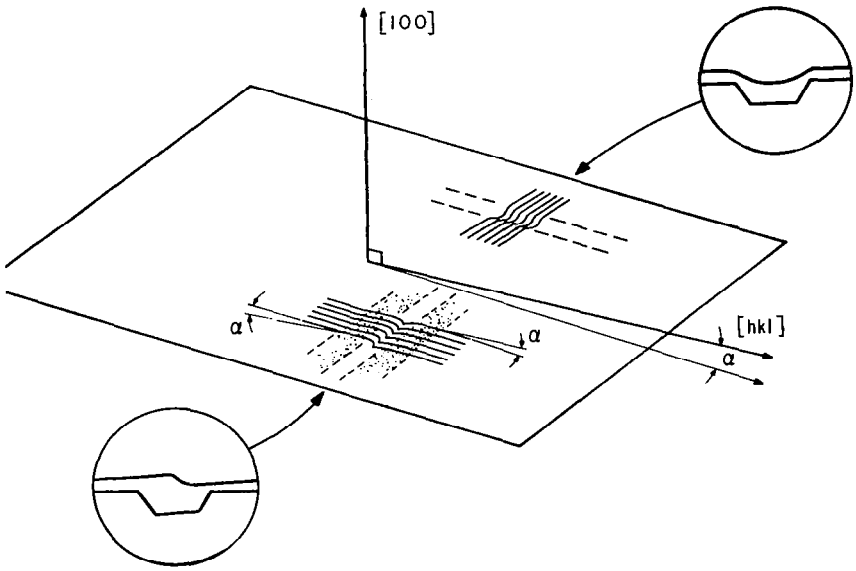

Figure 9. Diagram showing the effects of substrate misorientation on liquid-phase epitaxy over channels. The substrate is misoriented α degrees off the (100) plane and toward the [hkl] direction.

Figure 10 shows typical cross sections of (a) a pair of dovetail channels originally etched into the substrate and (b) a four-layer CDH structure. With the exception of the active layer, the grown layers' geometries are evident from Figure 10. Those layers, which are always thicker than ∿0.5 μm, follow the LPE growth dependence on surface curvature that we discussed in Subsection II.A. That is, enhanced growth in concave parts of the surface and dissolution and/or reduced growth in convex parts of the surface. The resultant layers (except the first layer and the active layer) have regions of minimum thickness above the mesa and taper sideways to larger thicknesses. We call this a leaky-guide shape (fig. 11). By contrast, the active layer, which is relatively thin ($\leq$0.2 μm), can be strongly influenced by the substrate misorientation and is much more sensitive to local surface curvature. As shown in Figure 9, when the substrate misorientation direction is parallel to the channel direction, the LPE growth is symmetrical. Otherwise, the presence of the channel triggers the formation of terraces (fig. 9) in what appears to be a tendency to reconstruct the low-surface-energy (100) plane (refs. 6,25). For thick layers, such terraces are reflected in some degree of asymmetry in layer

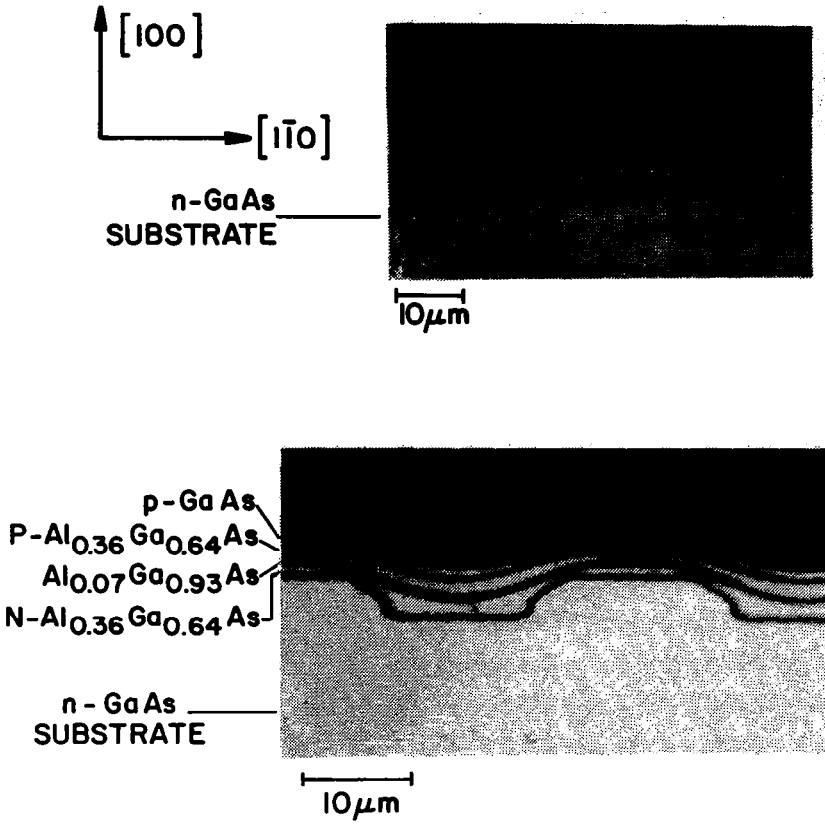

Figure 10. Top photomicrograph: cross section of a pair of dovetail-shaped channels. Bottom photomicrograph: lightly etched cross section of typical CDH structure. See Figure 11 for the active-layer-thickness variation above the mesa.

cross section (ref. 25). For thin layers, however, the effects of misorientation can be quite dramatic. Thus, as shown in Figure 11, when the substrate misorientation is 1 to 2° off (100) toward [010], the active-layer thickness decreases to one side while increasing to the other side. This semileaky-guide shape is a direct result of the crystal tendency to reconstruct the (100) plane. When the misorientation direction is parallel to the channels' direction (bottom of fig. 11), the active layer takes a symmetrical shape of the ridge-guide type due to reduced growth over the shoulders of the residual n-AlGaAs mesa (see fig. 2c). The two active-layer shapes, semileaky guide and ridge guide, are largely responsible for lateral mode control in most CDH lasers. We

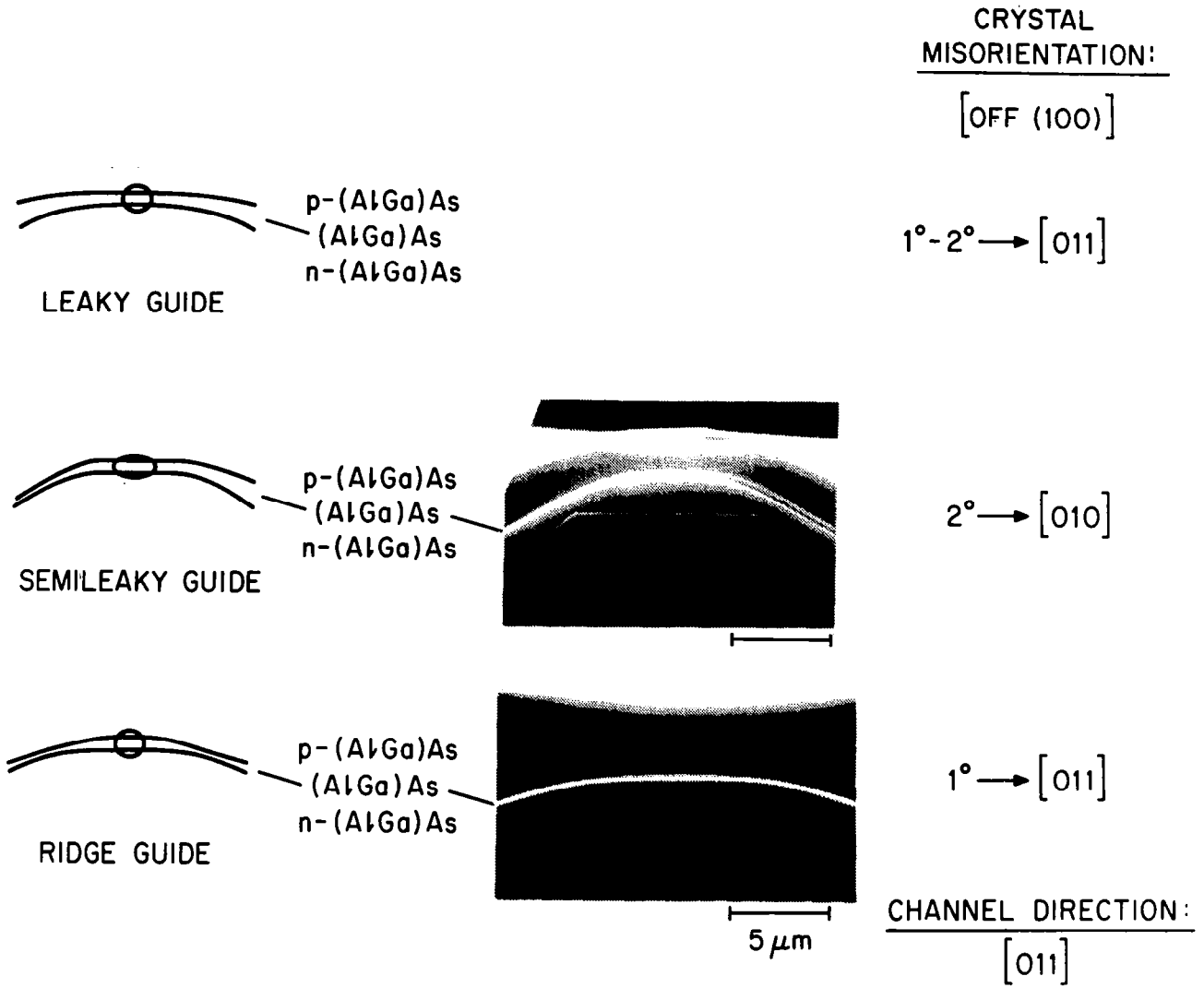

Figure 11. Types of CDH structures according to their active-layer-thickness variation. Leaky-guide devices could only be obtained above a channel shoulder (ref. 9). The active layers above the mesa are shown in scanning-electron-microscope photographs for both semileaky and ridge-guide devices.

have never encountered above the mesa a leaky-guide shape for the active layer. Leaky-guide active layers have only been obtained over channel shoulders (ref. 9) (see leaky-guide CDH structure in fig. 5c).

The CDH structure shown in Figure 10b has a relatively thin cap ($\sim$0.3 μm) in the region above the mesa. The structure's top surface has two residual channels and a residual mesa. If the p-AlGaAs layer and, expecially, the "cap" p^+-GaAs layer are grown thicker ($\sim$1 to 1.5 μm each), the resulting CDH structure (fig. 12) has no evidence of channels on its top surface. Instead a very shallow valley is obtained due to delayed growth over the mesa as compared to the planar regions. The resulting flat-top-surface geometry assures low thermal resistance values when the devices are bonded with indium solder, in very much the same manner as for buried heterostructures (ref. 43).

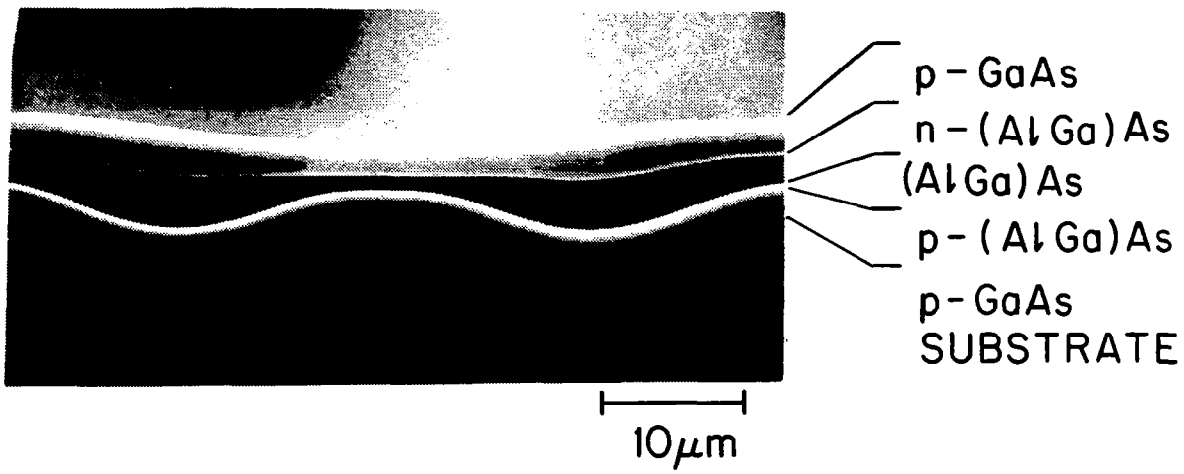

Figure 12. SEM photograph of the lightly etched cross section of a ridge-guide device with virtually flat top surface.

IV. RIDGE-GUIDE CDH LASERS

The schematic representation of a CDH laser of the ridge-guide type was shown in Figure 1a. Basically, the lateral mode confinement is provided by a local increase in active-layer thickness. As mentioned in the previous section, in order to obtain a symmetrical structure it is very important that the substrate misorientation direction be parallel to the channels' direction. An angle-lapped (5°) section illustrating the geometry of active layers in ridge-guide CDH devices is shown in Figure 13. The active layer (arched, dark stripe

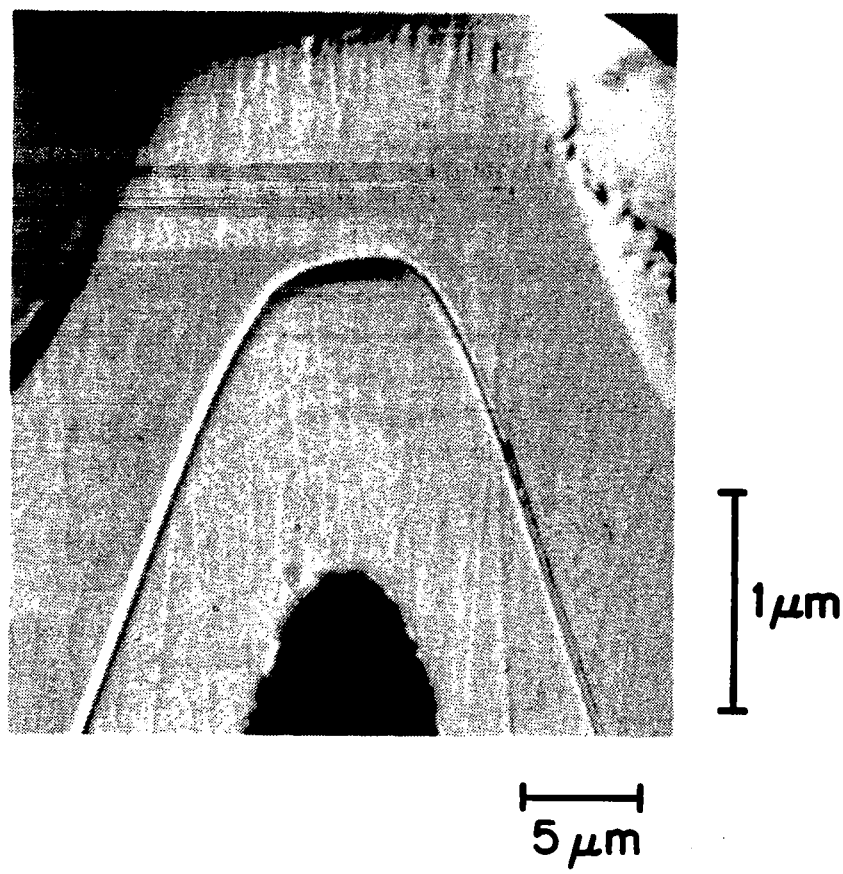

Figure 13. Photomicrograph of angle-lapped (5°), lightly etched cross section of ridge-guide CDH device. The arched, dark stripe in the center of the photograph is the active layer that tapers from a maximum thickness of 0.12 μm to 0.07 μm on either side.

in the center) has a maximum thickness of 0.12 μm. For over 3.8 μm in the lateral direction the thickness is more or less constant, and then it tapers down sharply to 0.07 μm for more than 1.5 μm on both sides. A positive-index cavity (fig. 4a) is thus formed. Below we present and discuss the electro-optical characteristics of such devices.

A. LIGHT-CURRENT CHARACTERISTICS

The current flow in a CDH device is shown schematically in Figure 14. The lasing spot size (2 to 3 μm) is determined by the ridge guide. The current is fed through a 10-μm-wide oxide-defined metallic stripe contact. Before reaching the active layer the current will spread laterally depending on the geometry and composition of the p^+-GaAs cap layer and the p-AlGaAs layer. For instance, a thick (1 to 1.5 μm) p^+-cap layer will cause considerably more current spreading than a thin (0.2 to 0.3 μm) cap layer (ref. 45). Thus, depending on the device structure, the current that goes into the lasing region, I_L, represents a smaller or a larger portion of the total current I. It must be stressed that the current not used in lasing ($I-I_L$) is radiative leakage current; that is, it recombines radiatively providing spontaneous emission. By contrast, the resistive-shunt leakage currents present in structures with discontinuous active layers (refs. 4,6,16,42 and fig. 7c) provide severe joule heating, which prevents cw operation. The radiative leakage current in the CDH device affects not only the total current, I_{th}, needed at lasing, but also the external differential quantum efficiency, η_{ext}, since of all carriers injected in the active layer only a fraction, $\eta_c = I_L/I$, participate in lasing (ref. 23). The η_{ext} formula is then:

$$\eta_{ext} = \eta_c \eta_{st} \frac{(I/L)\ln(1/R)}{\alpha_i + (1/L)\ln(1/R)} \tag{5}$$

where η_{st} is the internal quantum efficiency in stimulated emission, α_i is the internal cavity loss, L is the cavity length, R is the geometric mean of the facet reflectivities, and η_c is the efficiency of current pumping. Thus, CDH devices with relatively large leakage currents will not only have large I_{th} values, but low η_{ext} values as well.

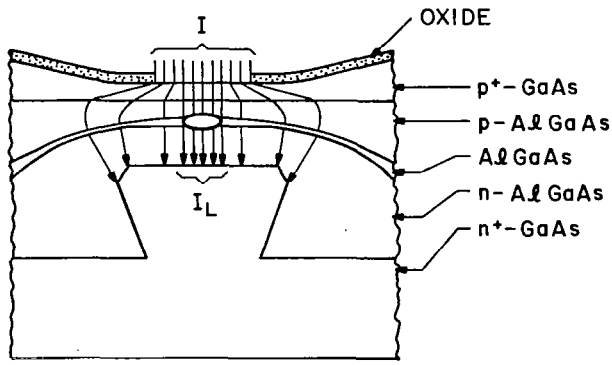

Figure 14. Schematic representation of current flow in the CDH device. The stripe contact has a nominal value of 10 μm. The current not participating in lasing, $I-I_L$, is radiative leakage current, unlike resistive-shunt currents in structures with discontinuous active layers (see fig. 7c).

Typical cases are shown in Figures 15a and b. Figure 15a depicts the cw L-I curves for 125-μm-long devices with thick (1.5 to 2 μm) p^+ capping layers. The six devices have remarkable reproducibility of their characteristics [I_{th} = 66 to 77 mA and η_{ext} = 11 to 13% (one facet)] considering that they have been randomly selected. For such devices the lasing spot size was about 3 μm wide. We estimate that only 25% of the total current goes into lasing. For comparison, we show in Figure 15b the L-I characteristics for a CDH device with a thin (0.2 to 0.3 μm) capping layer and a n^+-GaAs buffer layer that "peaks" above the mesa (ref. 18). For a similar device length (L = 100 μm) the threshold is 28 mA, and the external differential quantum efficiency is 27%. Thus, by simply growing a structure where the current spreading is minimized, the threshold was halved and the efficiency more than doubled. For this low-threshold CDH device we estimate that 40 to 50% of the current is used in lasing. The estimate is based on two sets of data: (1) threshold current vs device length (fig. 16a) and (2) external differential quantum efficiency vs device length (fig. 16b). The threshold current for uncoated devices varies almost linearly from 32 to 130 mA as the diodes' length is increased from 100 to 600 μm. Each data point corresponds to the spread in threshold for 7 to 10 devices at a given length. For the same device length we compare our results to threshold data from

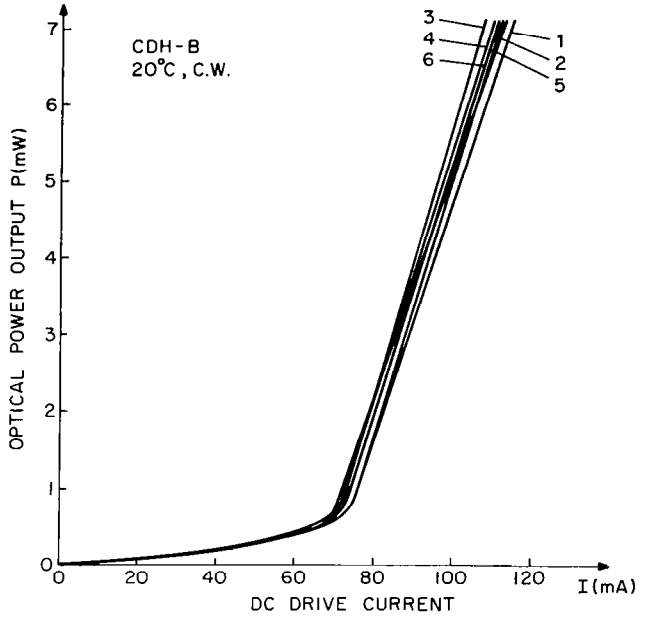

(a)

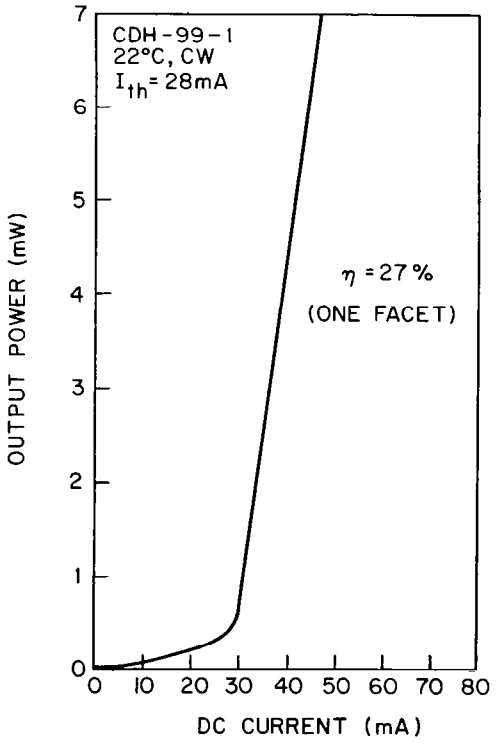

(b)

Figure 15. Typical cw light-current characteristics for ridge-guide CDH devices of (a) thick (1.5 to 2 μm) p^+-GaAs capping layer and (b) thin (0.2 to 0.3 μm) p^+-GaAs capping layer. Device lengths are 125 and 100 μm, respectively.

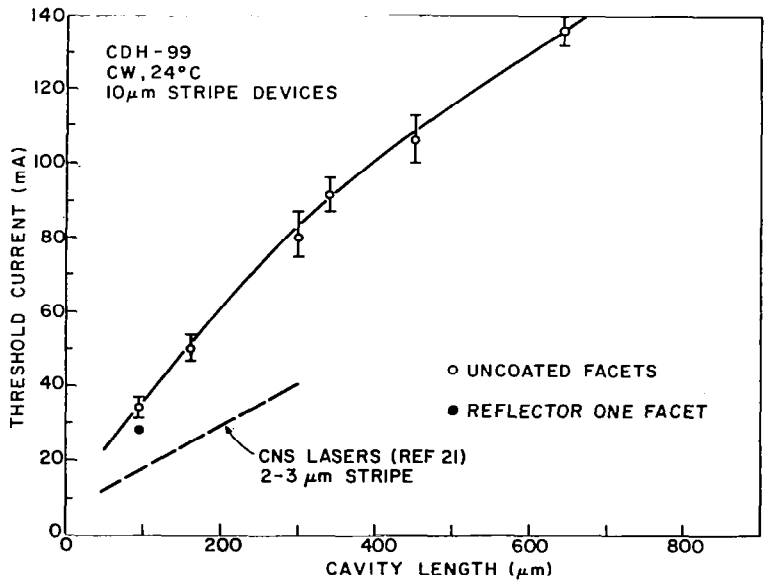

(a)

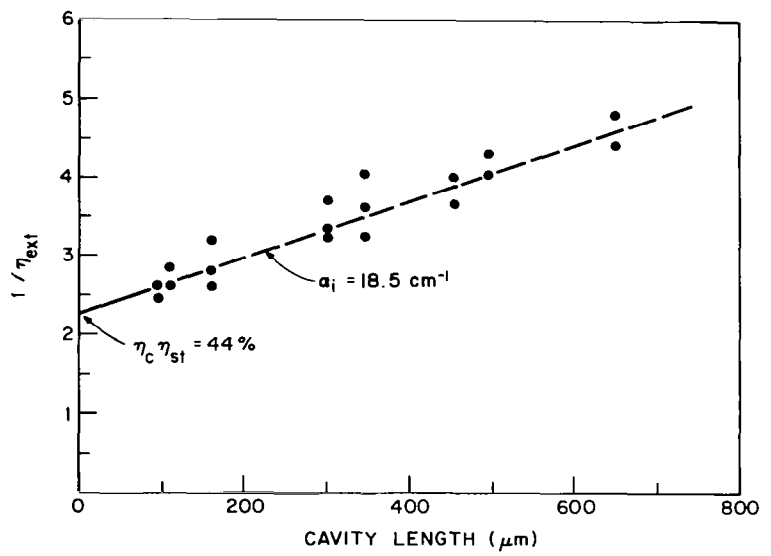

(b)

Figure 16. (a) cw threshold current vs device length for uncoated CDH devices and for CDH device with a reflector on the rear facet. The contact stripe width is 10 μm. The dashed line shows the I_{th} vs L variation for CNS devices (ref. 21) of 2- to 3-μm-wide stripes. For both CNS and CDH devices, the lasing spot is 2 to 3 μm wide ($1/e^2$ points in intensity). (b) Reciprocal of external differential quantum efficiency vs cavity length for uncoated ridge-guide devices. The product of the current-pumping efficiency and the internal quantum efficiency in stimulated emission is ∿0.44. The internal cavity loss is ∿18.5 cm^{-1}.

nonplanar-substrate devices of similar spot size but of tight-current confinement, i.e., 2- to 3-μm-wide stripes (refs. 21,22), and then it follows that only 40 to 50% of our current feeds the lasing area (see fig. 16a). The rest of the current is radiative leakage current. Further proof is obtained from the η_{ext} vs L data (pulsed operation). We plot $1/\eta_{ext}$ as a function of cavity length. The intercept with the vertical axis gives a value of 0.44 for the product of $\eta_c \eta_{st}$ and an internal cavity loss factor $\alpha_i \simeq 18.5\ cm^{-1}$. Since GaAs has an internal quantum efficiency close to unity, it follows that the intercept of the $1/\eta_{ext}$ line with the vertical axis gives $1/\eta_c$. The value thus obtained, 44%, agrees with the η_c estimate from I_{th} vs L data. As discussed below, the variation with temperature of the radiative leakage current gives extremely low temperature sensitivity for the threshold current.

B. NEAR-, FAR-FIELD, AND SPECTRAL CHARACTERISTICS

The size of the lasing spot is laterally determined by the built-in dielectric ridge guide. Due to its focusing properties, the ridge guide provides relatively small spots: 2 to 3 μm at $1/e^2$ points in intensity. In Figure 17 we show a typical near-field photograph and profile. The mode width at $1/e^2$ points in intensity is $\simeq$2 μm. Perpendicular to the junction, the lasing spot is $\simeq$0.6 μm wide as determined by the active and confinement layers, (ref. 46), but in Figure 17 it appears wider as limited by the resolution of the optical microscope. The lasing spot is always focused on the emitting facet as expected for real-index-waveguided lasing modes. The consequent lack of astigmatism combined with a relatively small spot size has allowed highly efficient coupling (60 to 70%) of ridge-guide CDH lasers to single-mode fibers of 4.5-μm-diameter core and 0.1 numerical aperture (ref. 47). (Up to 4-mW optical power was coupled into the single-mode fiber.)

Typical lateral far-field profiles and spectra are shown in Figures 18 and 19. When in fundamental-mode operation, the beam full width at half power, $\theta_{||}$ (FWHP), is generally found to follow the Gaussian-beam formula as related to the mode spot size:

$$\theta_{||} = 2 \arctan \frac{0.59\ \lambda}{\pi\ w_o} \qquad (6)$$

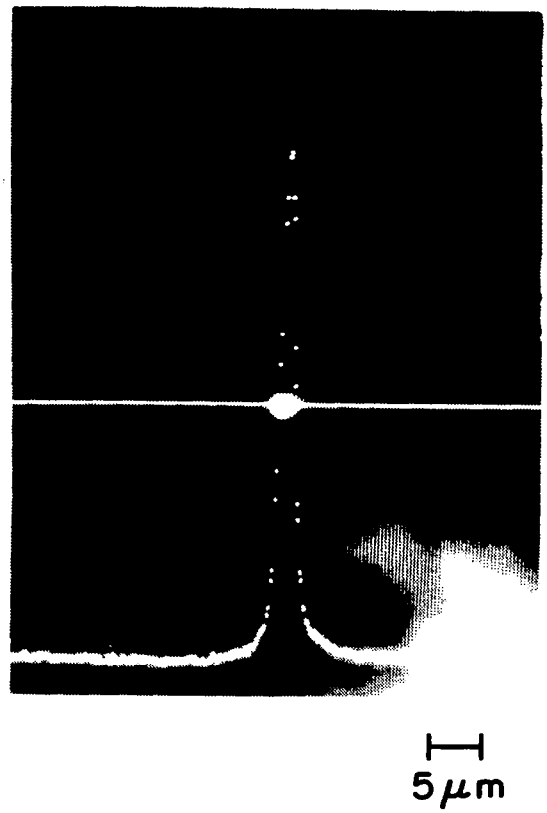

Figure 17. Near-field photograph and intensity profile (plane of the junction) of the lasing spot in ridge-guide devices.

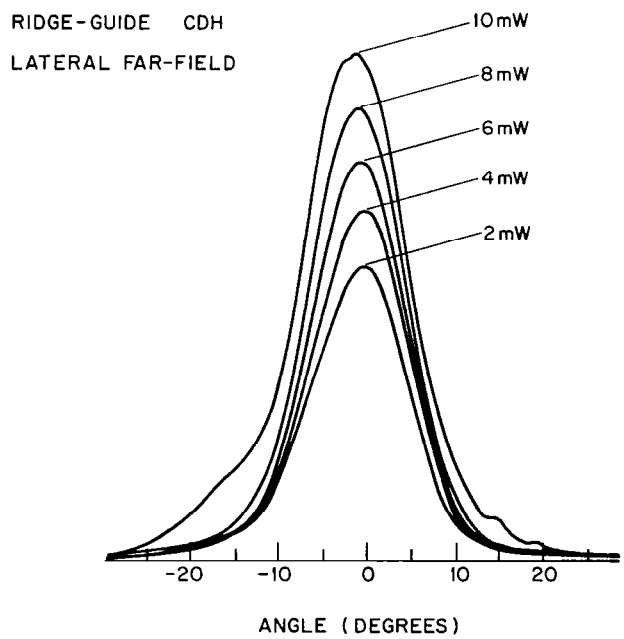

Figure 18. Typical lateral far-field patterns of ridge-guide device at various output power levels.

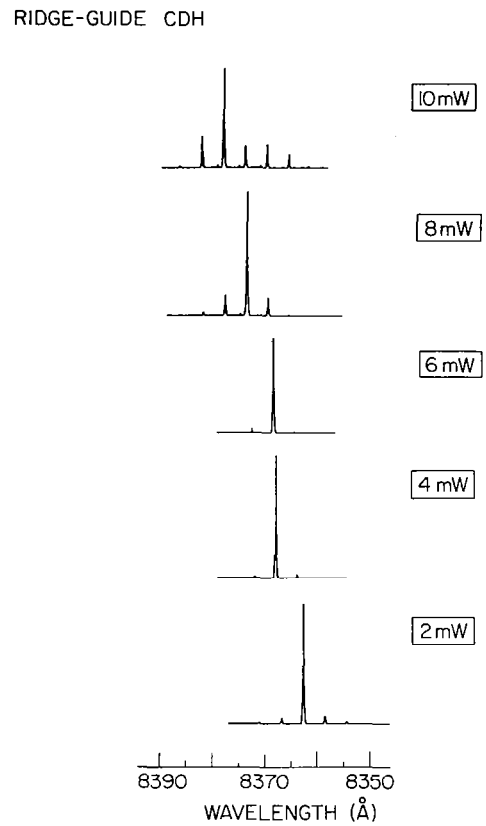

Figure 19. Spectrum of ridge-guide device at cw power levels up to 10 mW/facet (twice above threshold). The spectrometer resolution is 0.15 Å.

where w_o is the near-field half-width at $1/e^2$ points in intensity. Thus, as the near-field full-width varies from 2 to 4 μm, $\theta_{||}$ assumes values between 18 and 9°, respectively. In general we obtain $\theta_{||}$ values in the 12 to 20° range. We show in Figure 18 the evolution of the lateral far-field profile of a ridge-guide CDH laser as the output power is varied from 2 to 10 mW. Up to 6 mW the beam patterns are identical, with a beamwidth of 13°. At 8 mW, $\theta_{||}$ is still 13°, but the tails of the pattern are slightly distorted, which is indicative of the lasing onset of the first-order mode (i.e., the first high-order lateral mode). At 10 mW the presence of the first-order mode is quite evident as $\theta_{||}$ has increased and the pattern shape is severely distorted. In the near-field, some pattern broadening is observed, but it is not clear which mode is which since the fundamental and first-(high)-order lateral modes are superposed.

The spectrum is virtually single-longitudinal mode (fig. 19) from 2 to 6 mW. It should be stressed that over 60% of all CDH devices oscillate in a single-longitudinal mode when the device lases in the fundamental spatial mode. The excitation of a higher-order spatial mode is indicated by the appearance of another family of longitudinal modes and multilongitudinal mode operation for a given spatial mode. That is observed in Figure 19 for power levels above 6 mW. Therefore, based on lateral far-field patterns (fig. 18) and spectra (fig. 19), one can conclude that the ridge-guide CDH device analyzed here operates single-mode up to ∿7 mW.

Typically, ridge-guide CDH devices of 10-μm-wide stripe contacts become multimode spatially somewhere in the 3- to 7-mW range, depending on the particular device geometry. The reasons for multimode operation are related to both the device geometry and the current flow pattern. If the ridge guide is small enough (i.e., a convex-lens-shaped guide, 2 to 3 μm wide), only the fundamental mode can be supported (ref. 15), and then excitation of high-order modes is not a problem. However, such waveguides are difficult to grow and even if grown, the resultant optical mode is rather small (1 to 1.5 μm wide). More commonly grown are wider ridge guides of 5 to 8 μm (refs. 13,18,21) for which one hopes that only the fundamental mode is excited. At several milliwatts, however, spatial hole-burning will favor the excitation of high-order spatial modes (ref. 48). A solution for higher-power single-mode operation is to create a narrow current distribution peaked in the vicinity of the fundamental mode (refs. 21,22). Thus, the excitation of the first-order mode is "pushed" to higher powers. For instance, in CNS-type devices (refs. 21,22) the current already has a tendency to be diverted away from the center of the ridge guide as a result of the channel geometry, and thus 2- to 3-μm-wide contact stripes are needed for lasers to oscillate in the fundamental mode to 3 to 5 mW. By contrast, in the CDH structure the current is relatively uniform in the center of the ridge guide and thus fundamental mode excitation is always the case even when using 10-μm-wide stripes. However, the power level to which single-mode operation is achieved can be as low as 3 mW and most probably can be improved by confining the current to stripe contacts narrower than 10 μm. In any event, for most optical communication applications a power level of 5 mW is sufficient. Even if higher single-mode powers were readily available, they may not be usable since for 2- to 3-μm-wide lasing spots, a power output of 5 mW is about the highest allowable for reliable cw operation (ref. 31).

C. DEVICE CHARACTERISTICS AS A FUNCTION OF HEAT-SINK TEMPERATURE

One of the most remarkable properties of ridge-guide CDH devices is their relative insensitivity to temperature variations (refs. 18,23). On one hand is extremely low temperature sensitivity of the threshold current and temperature-invariant η_{ext} up to 100°C, and on the other hand the capability of such devices to lase to the highest ambient temperatures ever achieved: 170°C cw and 280°C pulsed. Such properties are directly attributable to the CDH geometry.

As shown in Figure 14, a large part of the total current I is "wasted" as radiative leakage current. The shape of the high-resistivity p-AlGaAs and n-AlGaAs layers as well as the presence of the high-conductivity n^+-GaAs substrate mesa will make the current concentrate in the region above the mesa and thus in the lasing region. As the heat-sink temperature is increased, the current needed for lasing increases, and lateral voltage differentials are created which further concentrate the current toward the mesa and the lasing spot. Thus, the ratio of the current going into lasing to the total current, I_L/I, increases with temperature (ref. 23). Then, while the threshold current density, J_{th}, will vary normally with increasing temperature (refs. 31,49), the total current at threshold, I_{th}, will vary with temperature considerably slower than J_{th}. The temperature dependence of the threshold current is represented by

$$I_{th}\,(T) = I_{th}\,(20°C)\,\exp\left(\frac{T - 20°C}{T_o}\right) \qquad (7)$$

where T_o is the characteristic temperature expressed in °C. For standard double-heterojunction lasers, T_o is found to be in the 150 to 200°C range over the temperature interval 20 to 70°C (ref. 31). By contrast, for CDH devices, T_o is found to be as high as 375°C at pulsed operation (ref. 23). That implies an I_{th} relative variation two to three times smaller than for any other practical AlGaAs DH lasers (refs. 21,31). Furthermore, in cw operation, where joule heating plays an important role, the I_{th} variation can be characterized by T_o values as high as 310°C. Typical results are shown in Figures 20 and 21. For the low-threshold device of Figure 20 the average threshold current variation with temperature is 0.2 mA/°C. The T_o parameters are evidenced when plotting the threshold current temperature variation on semilogarithmic graphs

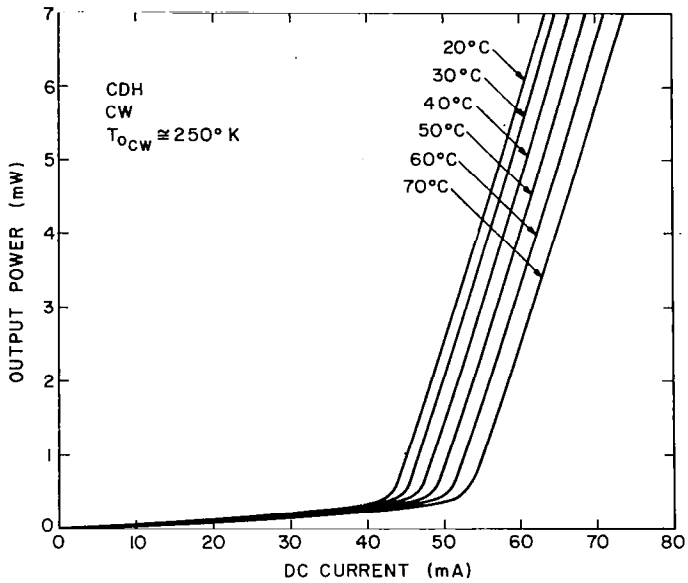

(a)

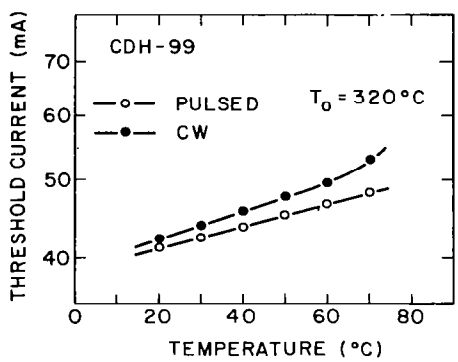

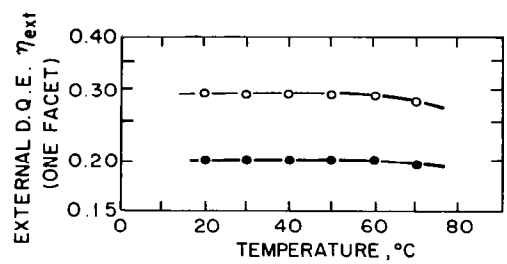

(b) (c)

Figure 20. (a) Typical light-current characteristics as a function of heat-sink temperature for low-threshold ridge-guide devices. (b) The variations of cw and pulsed lasing thresholds between 20 and 70°C. (c) The variations of the cw and pulsed external differential quantum efficiencies.

(figs. 20b and 21b). Again it should be mentioned that these T_o values characterize I_{th} and not J_{th}. The threshold current density varies normally with temperature (T_o = 160 to 195°C) as for broad-area lasers (ref. 23).

Another notable property is the virtual temperature invariance of η_{ext} (see figs. 20c and 21c). That is to be compared to steady decreases of η_{ext} with temperature (pulsed operation) for most types of AlGaAs lasers. While for CDH devices η_{ext} is constant from 20 to 100°C (ref. 50), for AlGaAs devices in general it is found that η_{ext} decreases by 30 to 35% over the same temperature

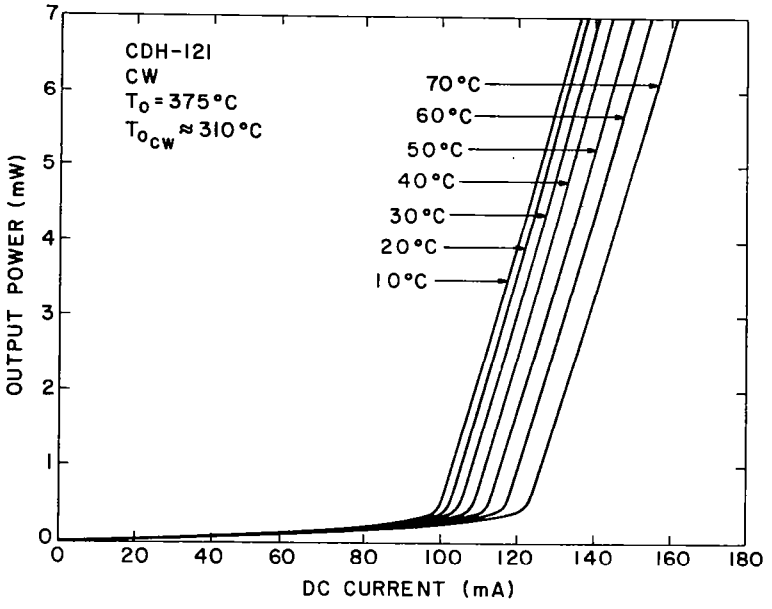

(a)

Figure 21. (a) Light-current characteristics as a function of temperature (20 to 70°C). The threshold-current coefficients T_o are 310 and 375°C in cw and pulsed operation, respectively. (b) Variations of the cw and pulsed threshold currents. (c) Relative variations in cw external differential quantum efficiency.

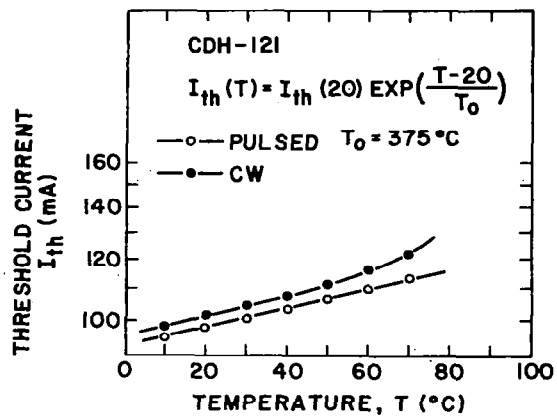

(b)

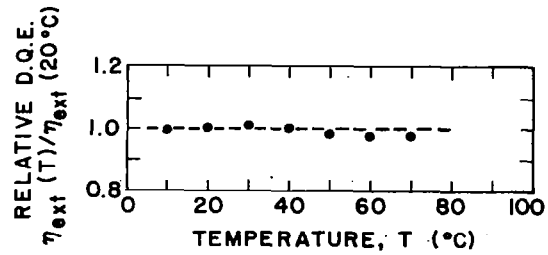

(c)

Figure 21. (Continued).

interval (refs. 21,50). The constancy of η_{ext} is attributable to the CDH geometry, since as shown in equation (5), η_{ext} contains the factor η_c which in turn is directly proportional to the ratio of lasing current to total current, I_L/I. Thus, as I_L/I increases with temperature, we expect a relative η_{ext} increase with temperature. That indeed happens when comparing the η_{ext} variation of CDH devices with the η_{ext} variation of broad-area diodes fabricated from the planar areas between CDH structures (ref. 23). While broad-area devices have a decrease of 20 to 30% in η_{ext} over the 20 to 70°C temperature interval, very similar to "standard" AlGaAs lasers, the η_{ext} of CDH devices remains virtually constant. A particularly relevant comparison is that between

CDH devices and CNS devices (ref. 21) with the same lasing spot size. In CNS devices most of the current feeds the lasing spot, which explains why their threshold currents are roughly half the threshold of CDH devices (see fig. 16a). Thus, one expects CNS devices to behave like broad-area lasers. Indeed for CNS devices (ref. 21), $T_o \simeq 180°C$ and η_{ext} decreases by 35% between 20 and 100°C.

It must be stressed that high-T_o, constant-η_{ext} behavior was obtained from most chips on a given wafer of ridge-guide CDH devices (ref. 23) and for all ridge-guide CDH wafers. This is in sharp contrast to the anomalous threshold-current temperature dependence reported for some proton-bombarded planar devices grown by molecular-beam epitaxy (ref. 51). While the heat-sink temperature was varied, we monitored the far-field pattern of several high-T_o devices. As shown in Figure 22, the lateral far-field pattern is found invariant to heat-sink temperature changes in both cw and pulsed conditions. This is of course expected if the lateral mode confinement is provided by a real-index dielectric waveguide (ref. 52) such as the ridge guide. Figure 22 also confirms that the high-T_o behavior of CDH devices is not related to lateral mode guiding.

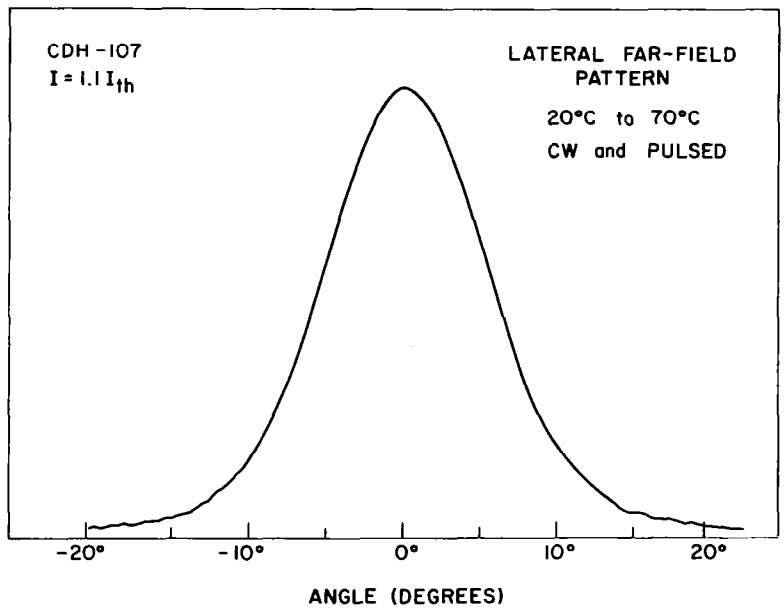

Figure 22. Typical lateral far-field pattern of high-T_o ridge-guide devices, cw and pulsed, from 20 to 70°C.

The fact that relatively low-threshold (30 to 50 mA) devices displayed very low temperature sensitivity of their threshold currents led us to study the behavior of CDH lasers at temperatures much higher than 70°C. The results are shown in Figures 23 to 25. Indium, which is commonly used for chip bonding,

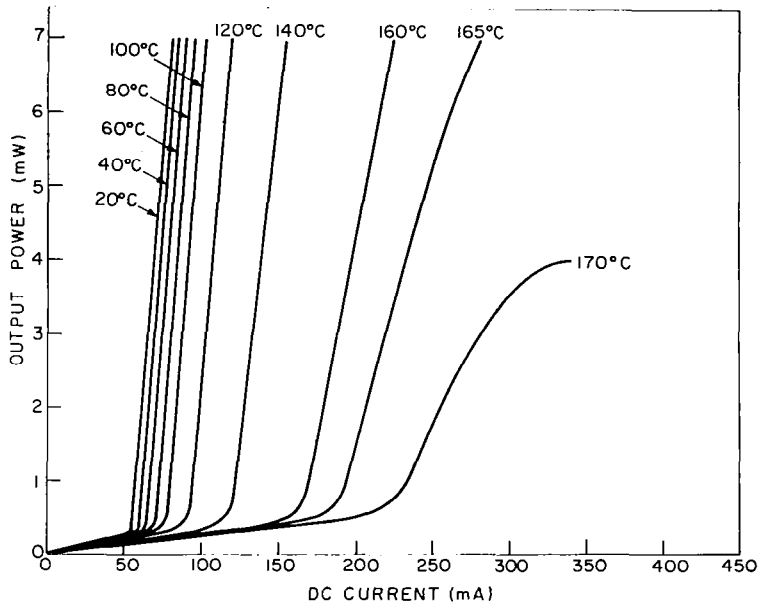

(a)

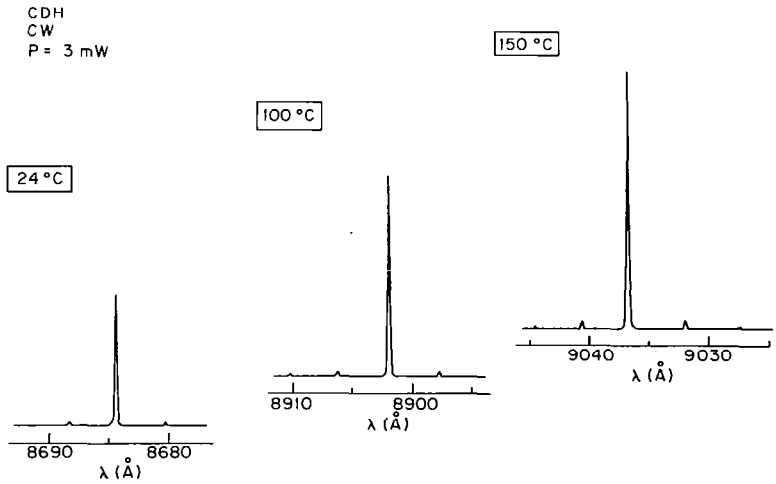

(b)

Figure 23. (a) cw light-current characteristics of ridge-guide device at various heat-sink temperatures. (b) Spectra of ridge-guide device at 3 mW/facet and various heat-sink temperatures. At 150°C and 3 mW, the junction temperature is ~170°C.

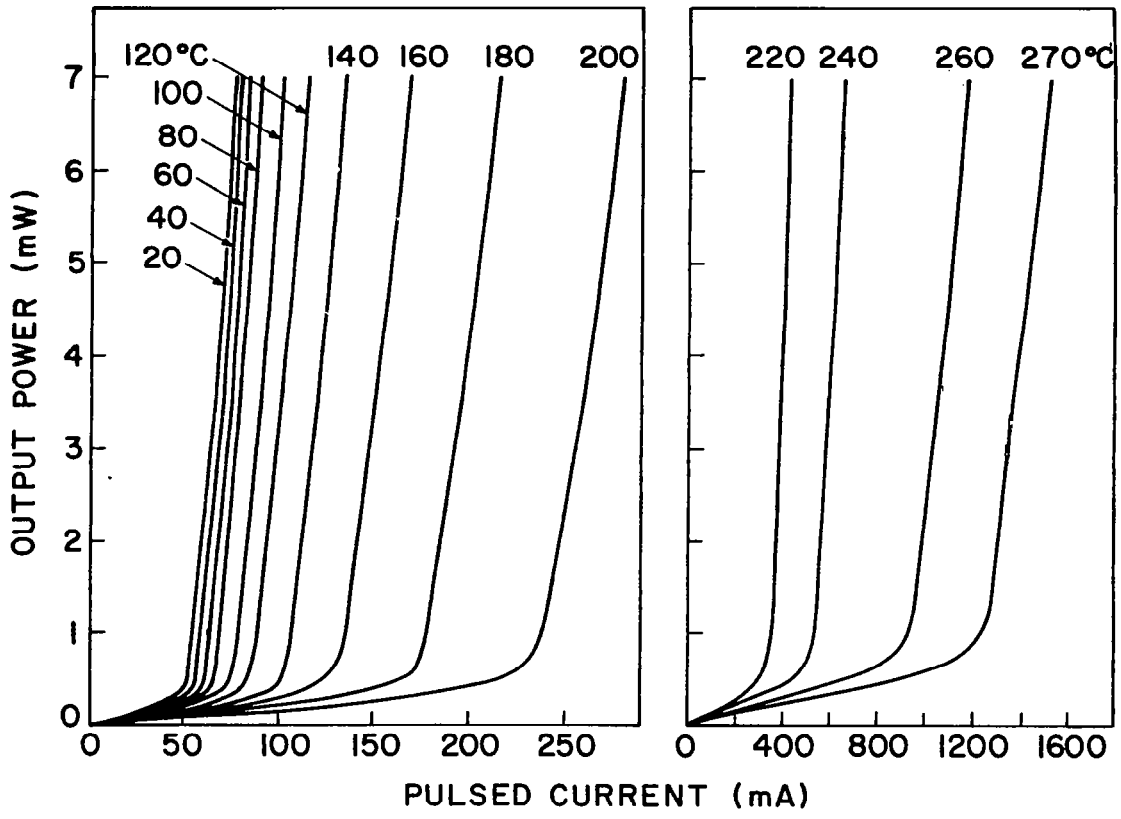

Figure 24. Typical pulsed light-current characteristics of ridge-guide devices at various heat-sink temperatures. At 280°C the threshold current is 1.5 A.

was replaced with Au-Sn solder of a much higher melting point (i.e., 280°C vs 156°C for In). In cw operation, lasing has been demonstrated (fig. 23a) to an ambient temperature of 170°C, which to the best of our knowledge is the highest temperature ever reported for cw diode laser operation. The devices employed were 250 μm long with dielectric-facet reflectors (ref. 53) on their rear facets. Single-mode cw operation (3-mW output power level) was recorded up to 150°C (fig. 23b). From pulsed and cw spectra we estimate that at a heat-sink temperature of 150°C and at 3-mW power level, the junction temperature is only 20°C higher. This relatively small temperature differential between the device junction and the heat-sink is mostly a reflection of low device thermal resistance values: 20 to 25°C/W as measured from shifts of the spontaneous emission

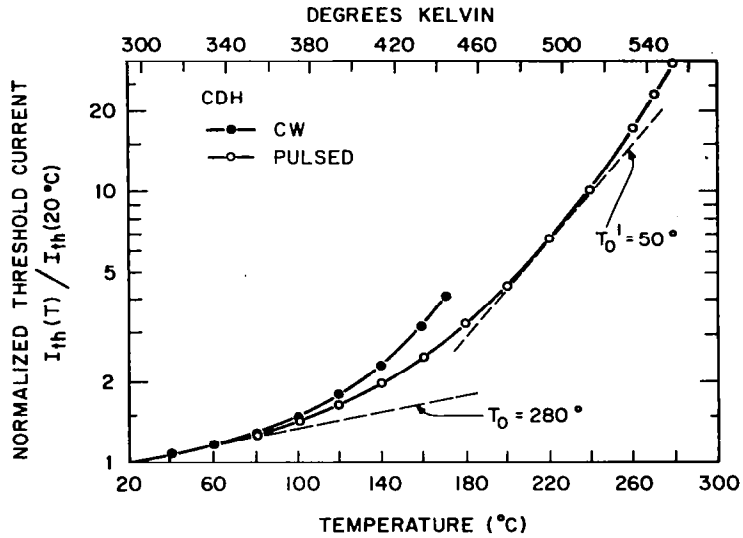

(a)

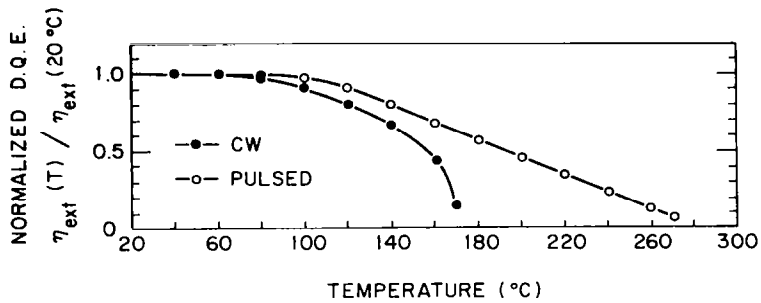

(b)

Figure 25. Relative variations with heat-sink temperature of (a) the cw and pulsed lasing thresholds (T_o and T_o' are temperature coefficients) and (b) the cw and pulsed external differential quantum efficiencies.

spectrum cw vs pulsed over the 20 to 100°C temperature interval. For 250-μm-long devices with 10-μm-wide stripes, thermal resistance values close to 20°C/W can only be explained if most of the spontaneous emission generated in the active layer is absorbed in the GaAs substrate and the p^+-GaAs capping layer. This so-called "radiative transfer" process (refs. 54-66) is dominant in the CDH device. On one hand an absorbing GaAs-substrate mesa is in close proximity (1 to 1.5 μm) to the layer, and on the other hand the thick n-AlGaAs layers on either side of the mesa prevent the generated heat from diffusing toward the active layer. We note that our thermal resistance results agree well with experimental data of Duda et al. (ref. 56) (65% radiative transfer of energy) and theoretical calculations by Newman et al. (ref. 55).

In pulsed operation the CDH lasers could be driven to temperatures as high as 280°C (figs. 24 and 25a) as limited by the melting point of the Au-Sn solder used (ref. 50). We show in Figures 25a and b the relative variations with heat-sink temperature of the threshold current (cw and pulsed). Up to 100°C there is almost no difference between cw and pulsed laser behavior, as a result of the low device thermal resistances mentioned above. The high-T_o, constant-η_{ext} behavior, however, is limited to temperatures below 100°C. From 125 to 160°C (cw operation) and from 120 to 200°C (pulsed operation), the threshold current and η_{ext} variation are very similar (ref. 50) to the variations reported by other researchers. Thus, we conclude that the current-concentration effect responsible for high-T_o behavior saturates around 100°C, where the current flow reaches a stable pattern. Therefore, above 120°C the relative variations of I_{th} can be considered to characterize J_{th} as well.

The most dramatic change in laser behavior occurs for temperatures above 180°C. The pulsed threshold current can be characterized by T_o values of 40 to 50°C from 180 to 260°C, and the (pulsed) spontaneous emission below threshold becomes increasingly sublinear as the temperature is raised above 220°C. (See ref. 50.) Both effects are believed (ref. 50) to reflect band-to-band Auger recombination; that is, the same nonradiative process currently proposed to explain InGaAsP/InP laser behavior around room temperature (ref. 57). In fact, it can be calculated* that for GaAs DH lasers at 500 K the Auger lifetime at threshold is ∿5 ns; that is comparable to the radiative lifetime (3 to 4 ns). Our results confirm these theoretical calculations.

*N. K. Dutta and J. R. Nelson, to be published in J. Appl. Phys.

D. MODULATION CHARACTERISTICS

Three laser modulation characteristics are of interest for optical communication applications: (a) the optical pulse response to an input current pulse, (b) the small-signal frequency response, and (c) the degree of harmonic distortion in the light-current curve.

Typical pulse response behavior is shown in Figure 26a. As the bias current, i_b, is increased relative to the threshold current, i_t, an evolution of the output light response occurs. As i_b approaches i_t, one can notice relaxation oscillations which are damped rather quickly (i.e., within 1 ns). For $i_b > i_t$, the pulse response shows no relaxation. The pulse response is thus quite similar to the ones reported for CSP (ref. 2) and BH lasers (ref. 58). It must be stressed that for CDH lasers, as for most other real-index guided lasers, we never observe self-pulsating behavior in unaged devices. This is our routine observation, and it has been independently confirmed by other researchers (ref. 59). One interesting feature is that the pulse response has a relatively slow turn-off as a function of bias level. The reason, just as in the case of CSP lasers, may be lateral carrier diffusion (refs. 60, 61). The "tailing" effect on the output response can cause intersymbol interference for data transmission rates above 200 Mbit/s.

In Figure 26b we show the pulse response under 450 Mbit/s operation (RZ and NRZ) as the bias current varies with respect to the threshold current. Best results are obtained when i_b is near or above i_t. CDH ridge-guide lasers have also been used in 500 Mbit/s transmission modules (ref. 47). These results demonstrate the capability of CDH lasers for high-data-rate transmission of optical information.

The frequency response to small-signal modulation is generally found (ref. 59) to show a relatively small resonance peak at $\sim$1 GHz, which shifts slowly with increasing current above threshold, as shown in Figure 27. The amplitude of the noise resonance decreases only slightly with increasing current,

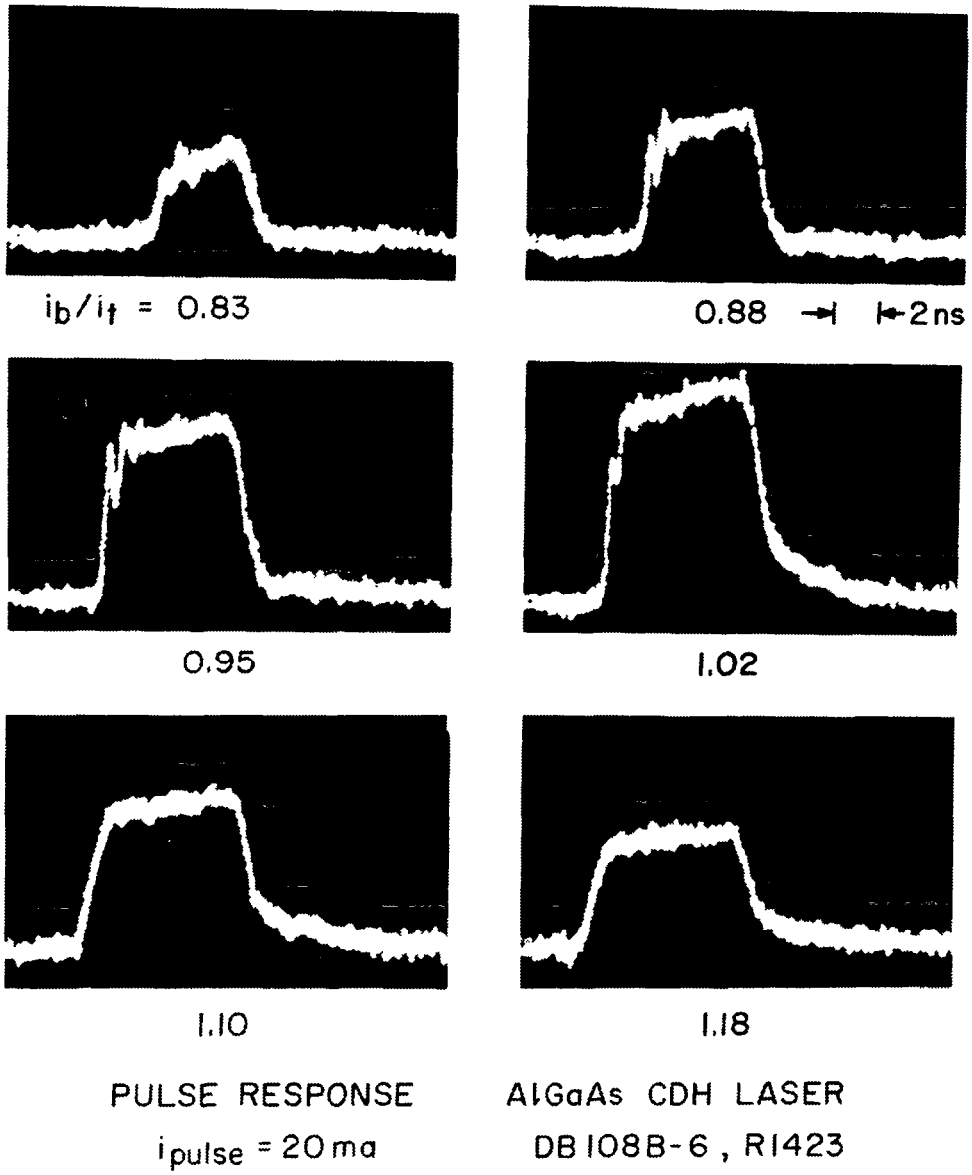

Figure 26. (a) Typical optical pulse response to input current pulses at several dc bias-current, i_b, levels with respect to the threshold current, i_t. (b) The pulse response under 450 Mbit/s operation in the RZ and NRZ conditions and at various bias current levels with respect to the threshold current.

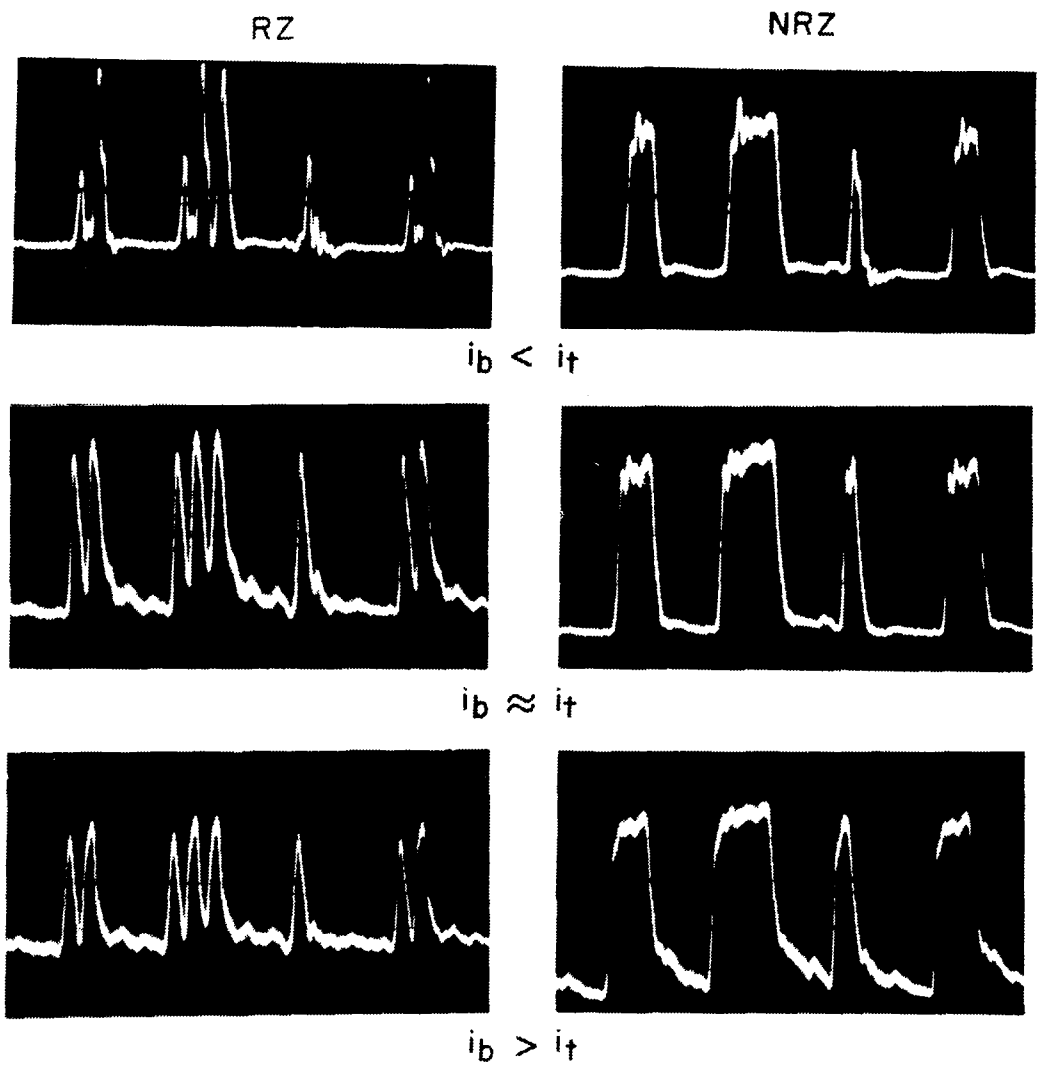

(b)

Figure 26. (Continued)

unlike CSP or BH lasers (ref. 59). The high degree of spatial mode stability in CDH lasers results in very linear light-current characteristics. Typical second-harmonic distortion characteristics for CDH devices under sinusoidal modulation are shown in Figures 28a and b. In Figure 28a, results of second-harmonic

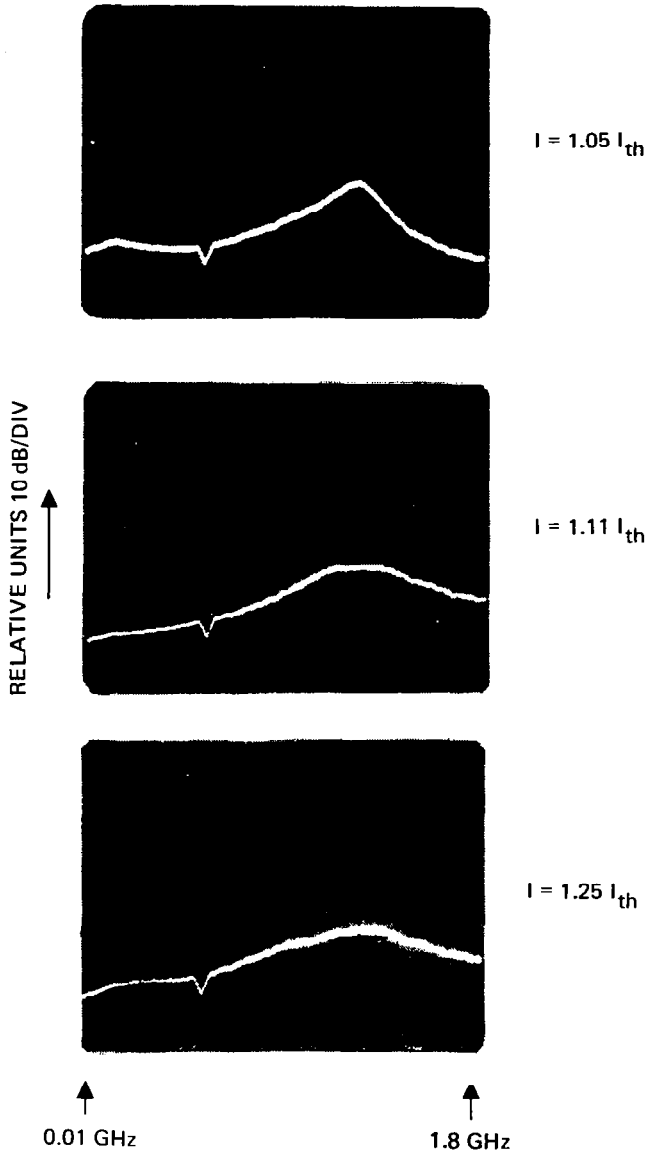

Figure 27. Typical light output vs frequency plots for ridge-guide CDH lasers at several current levels above threshold. After Figueroa (ref. 59).

distortion are shown at various bias current levels above threshold as the modulation current amplitude (peak-to-peak) is kept constant at 10 mA, and the modulation frequency is 100 MHz. As the bias level is increased above threshold, the second-harmonic distortion drops to the -50 dB level below the fundamental level at $i_b \simeq 1.12\ i_t$ and at a corresponding output power level of

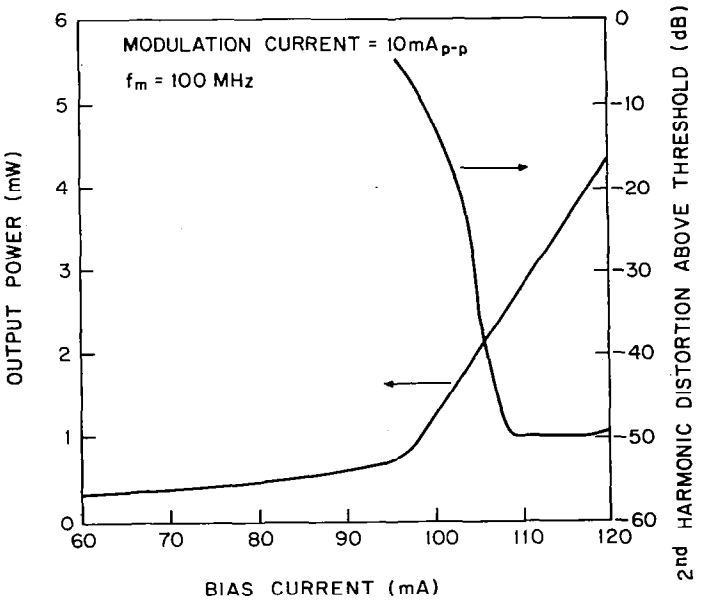

(a)

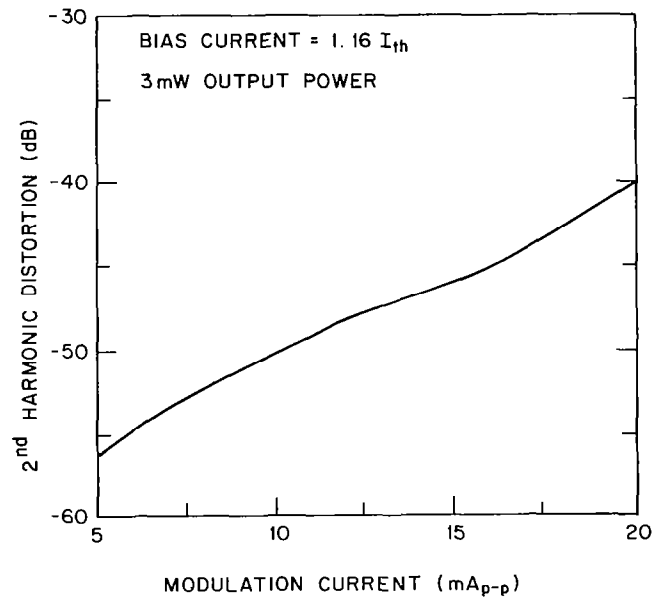

(b)

Figure 28. Second-harmonic distortion characteristics in CDH lasers under sinusoidal modulation: (a) at various bias levels above threshold, while the peak-to-peak amplitude of the modulation current is kept at 10 mA and (b) at a fixed bias level, while the peak-to-peak amplitude of the modulation current is varied.

2.5 mW. Further increase in bias current gives the same amount of harmonic distortion (i.e., -50 dB) up to the 4.5-mW output power level. Another experiment consists of keeping a constant bias current level ($i_b = 1.16\ i_t$) while varying the amplitude (peak-to-peak) of the modulation signal. The output power was 3 mW. As the modulation current is varied from 5 to 20 mA_{p-p}, the second-harmonic distortion varies from -57 to -40 dB. Both harmonic distortion results are comparable to the best results reported for buried-optical-guide (BOG) lasers (ref. 58) and plano-convex-waveguide (PCW) lasers (ref. 12). The excellent linearity of CDH lasers makes them quite suitable for analog communication systems.

V. SEMILEAKY CDH LASERS

The semileaky type of CDH device is schematically shown in Figure 1b, and a typical active-layer-thickness variation is shown in Figure 11. Basically the active layer has a central portion of constant thickness, tapers to one side to smaller thicknesses, and tapers to the opposite side to larger thicknesses. As discussed earlier (Section II.B), this asymmetrical structure provides total internal reflection to one side, just as in ridge-guide devices (i.e., guiding), and partial reflection together with radiation leakage to the other side (i.e., antiguiding). Below we discuss the structure's antiguiding nature and present typical electro-optical characteristics.

A. ANTIGUIDING NATURE

Semileaky-guide CDH lasers are grown on substrates misoriented 1 to 2° off (100) toward [010], and thus the substrate misorientation direction is at 45° with respect to the channels' direction. As a result of the crystal growth tendency to reconstruct the low-surface-energy (100) plane, a laterally asymmetrical active layer is obtained. The structure is a "leaky" guide or antiguide since the optical mode is only partially confined as a result of an increase in N_{eff} to the side where the active-layer thickness increases. The "leaked" radiation can be observed in the near-field profile below threshold (fig. 29a) and in the lateral far-field profile (fig. 29b). Below lasing threshold, light generated and guided in the constant-thickness region of the active layer leaks to the side where the active-layer thickness increases. All spatial modes are excited such that the near-field intensity profile is a convolution of all modes, leaky and nonleaky, and thus quantitative estimates are not possible. However, the strong asymmetry displayed is an indication of the leaky nature of the structure to one side. Lasing occurs in a relatively large spot: 3.5 to 5.0 μm at $1/e^2$ points in intensity, depending on the geometry (refs. 1,10). While the lasing near-field profile is found to be virtually symmetrical (ref. 10), the lateral far-field pattern is always asymmetrical and displays a sidelobe at 13 to 20° with respect to the main lobe. As discussed below, these are telltale signs of radiation leakage.

When one considers a step-index antiguide mode (see bottom right corner of Fig. 6), the leaked radiation, α_R, will emerge at an angle θ with respect to the laser axis (inside the semiconductor) (ref. 62) where

$$\sin \theta = \sqrt{\frac{2|\Delta n|}{n_o}} \tag{8}$$

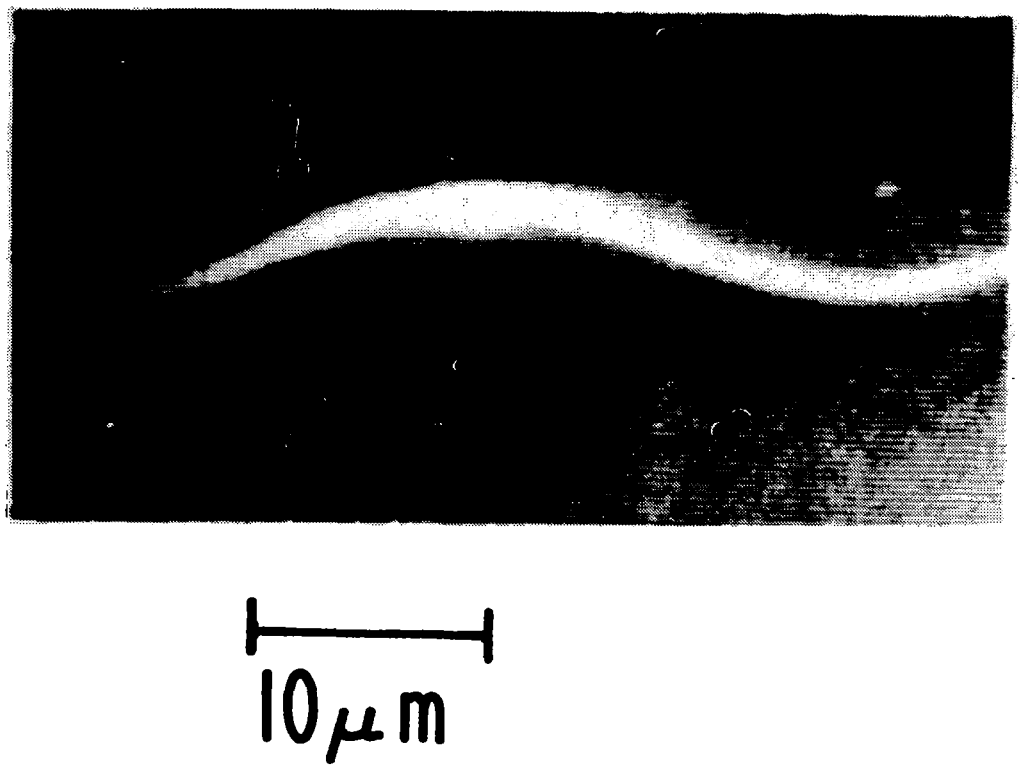

(a)

Figure 29. Semileaky-guide CDH laser: (a) typical near-field intensity pattern close to but below threshold and (b) typical lateral far-field patterns at output powers up to 10 mW/facet.

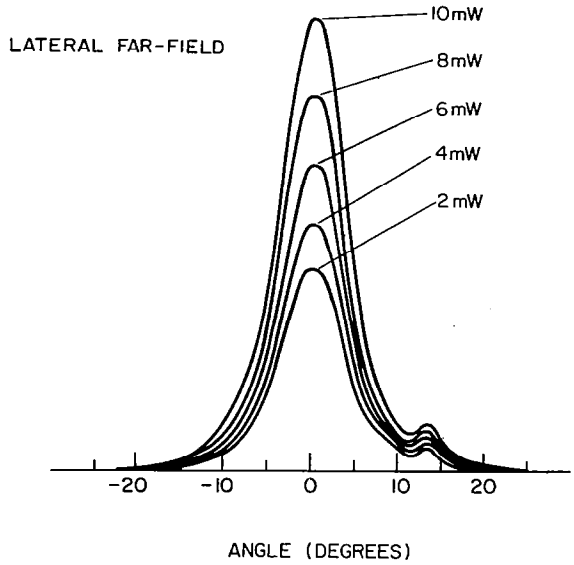

(b)

Figure 29. (Continued)

For $n_o = 3.6$ and $|\Delta n| = 0.01$ we obtain $\theta = 4.3°$. Upon refraction at the semiconductor-air interface, the leaked radiation should be observed in the far-field at an angle θ_R:

$$\theta_R = \text{arc sin } (n_o \sin \theta) = \text{arc sin } \sqrt{2n_o|\Delta n|} \tag{9}$$

For the same case, $\theta_R = 15.5°$. Experimentally we have observed a faint peak, only to one side, at 13° with respect to the main lobe (fig. 29b), while the main lobe has a full width at half maximum of 8°. The weakness of the side peak can be understood as a result of heavy absorption of the leaked radiation in the active layer. For some devices the side peak was hardly noticeable, although the far-field and near-field patterns were asymmetric (ref. 10). Even though small, the asymmetries in the far-field and near-field profiles, especially below threshold (fig. 29 and ref. 10), bring strong supporting evidence to the semileaky-guide model. Further evidence is the difference in single-mode behavior compared to that of a ridge-guide device; that is, lasing in larger spots due to the defocusing properties of the semileaky cavity and lasing to higher power levels due to mode-dependent losses in the semileaky cavity. As calculated in Subsection II.B, the radiation losses for the fundamental mode of a typical semileaky structure have reasonable values (i.e., 10 to 20 cm^{-1}) when compared to standard values for cavity losses of a diode laser

(60 to 90 cm^{-1} for mirror and free-carrier loss). By contrast, according to equation (4), α_R for the first-order mode will be four times the radiation loss for the fundamental mode and thus higher-order mode operation will not occur until the current reaches 1.5 to 2 times the threshold of the fundamental mode. The experimental results presented below confirm this.

B. LIGHT-CURRENT AND SPECTRAL CHARACTERISTICS

Typical cw light-current characteristics are shown in Figure 30. At 20°C the device has a "kinkless" characteristic up to catastrophic damage levels: 30 mW/facet. However, the device is single-mode only up to 12 mW. Above 12 mW higher-order spatial modes are excited that share the power with the fundamental mode. The transition from single to multimode behavior is not noticeable with a large-area detector and thus the L-I curve does not show "kinks." In general, we have achieved single-mode operation up to twice the threshold current value

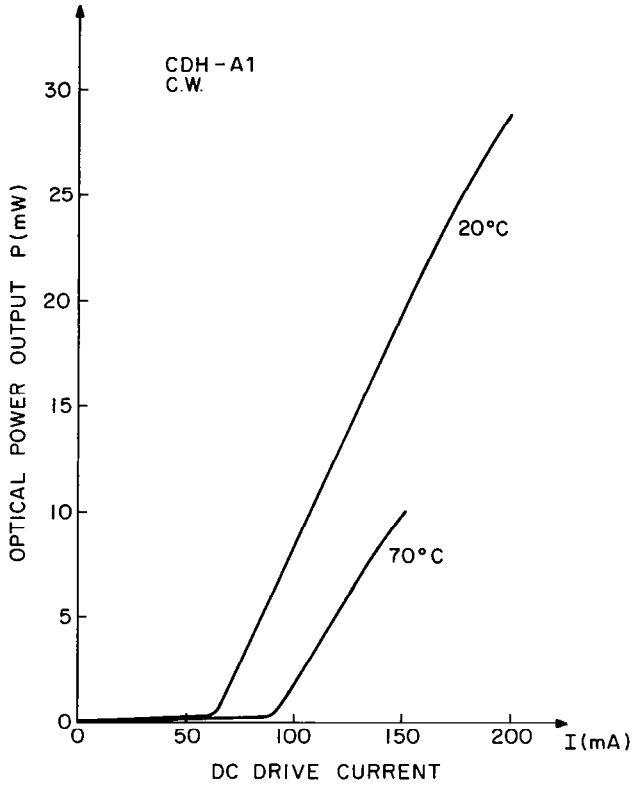

Figure 30. Typical cw light-current characteristics of semileaky-guide CDH lasers at 20 and 70°C (ambient temperature).

and up to 10 to 15 mW/facet. These figures are to be compared to 3 to 7 mW/facet single-mode operation for ridge-guide devices. At 70°C in cw operation the semileaky diode was driven "kinkless" to 10 mW/facet. The T_{ocw} is 150°C, much less than for ridge-guide devices. The difference may arise from the built-in asymmetry of the structure, which in turn affects how the current flow pattern varies with heat-sink temperature and/or may be related to the leaky nature of the device.

The cw spectrum for a typical semileaky CDH device is shown in Figure 31. The device oscillates multimode longitudinally up to 2 mW/facet and then becomes single-mode up to twice above threshold, where the power level is 10 mW/facet. This is a typical maximum power of single-mode operation for semileaky-guide lasers. Single-mode operation to powers as high as 15 mW/facet have been measured (ref. 1). The linewidth is less than the spectrometer resolution (i.e., <0.15 Å). The modulation characteristics are the same as for ridge-guide devices.

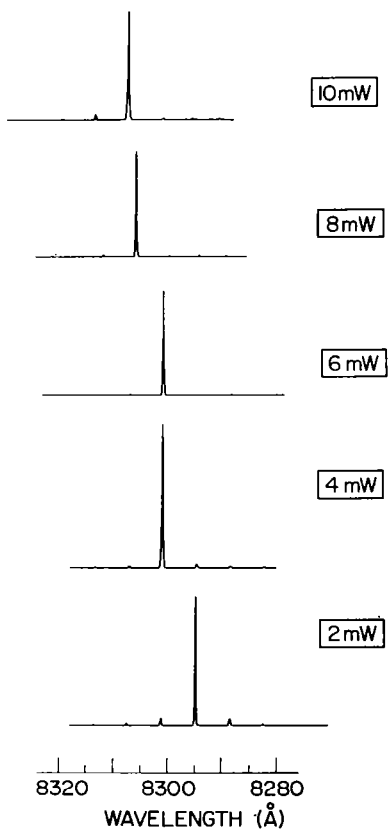

Figure 31. Typical spectra for semileaky-guide CDH lasers at various output power levels. At 10 mW/facet the device is biased at twice threshold. The spectrometer resolution is 0.15 Å.

C. THIN-ACTIVE-LAYER STRUCTURES

As mentioned previously the power level for reliable operation is mainly determined by the size of the lasing spot (ref. 31). One approach to increasing the spot size is to grow structures of very thin ($d < 0.1$ μm) active layers. While for $d = 0.15$ to 0.2 μm (typical values for the central portion of semi-leaky lasers), the mode width is 0.5 to 0.6 μm, for 0.05- to 0.06-μm-thick active layers the mode width reaches values around 1 μm (ref. 46). In an effort to achieve high-power CDH devices we have grown (ref. 63) semileaky devices of very thin active layers. A typical active-layer angle-lapped cross section is shown in Figure 32. The central portion is ~600 Å thick and tapers sideways to less than 500 Å to one side and 900 Å to the other side. The very thin nature of the active layers was reflected in transverse beams of relatively narrow full-width at half-power (ref. 63): $\theta_{\perp} = 27$ to 30°. The spot size increased not only perpendicular to the junction but also in the plane of the junction. Thus, mode lateral widths of $\sim$7 μm ($1/e^2$ points in intensity) were obtained as opposed to 3.5 to 5 μm for regular semileaky devices. The reason for a larger spot size is believed to be a result of the nearly planar active-layer geometry (fig. 32) as well as strong antiguiding.

Single-mode cw operation was achieved up to 21 mW/facet with threshold currents in the 100- to 150-mA range for 150-μm-long devices (ref. 63). Particularly relevant for the device's antiguiding nature and high-power capability are the lateral far-field patterns at various output power levels (fig. 33). The device operates single-mode to 50 mW/facet at 50% duty cycle (50-ns-wide pulses and 10-MHz repetition rate) (fig. 33). The far-field is asymmetrical and it displays some structure, especially at low powers. We believe that such far-fields are a convolution of the leaked wave and of the wave confined to the center of the semileaky guide. In fact, the main lobe may well correspond to the leaked radiation, in the same manner as the far-field patterns calculated by Streifer et al. (ref. 64) for asymmetric antiguiding structures.

A slight peak shift (~2°) is noted as the laser is driven from 10 to 50 mW. This is consistent with the antiguiding model (fig. 6). As the drive level is increased under near-cw condition, the amount of local heating increases. Since heating has a positive contribution to the index of refraction, it follows that the net index depression $|\Delta n|$ is lowered, which in turn strongly

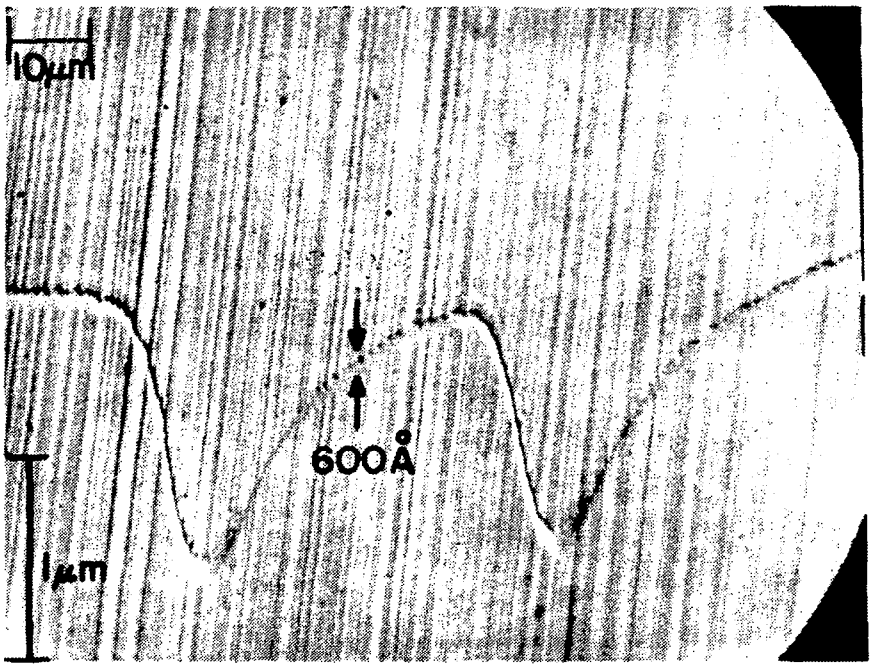

Figure 32. Photomicrograph of angle-lapped (2°), lightly etched cross section of thin-active-layer semileaky-guide device. The central part displays the lateral thickness variation of the active layer.

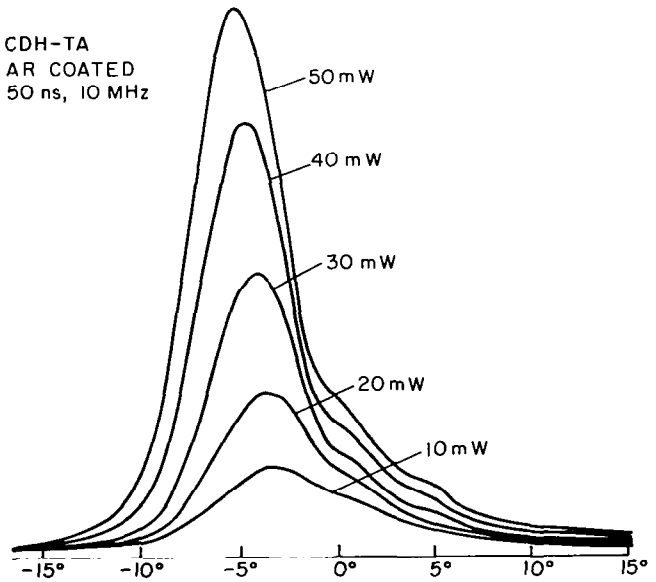

Figure 33. Lateral far-field patterns of thin-active-layer semileaky laser from 10 to 50 mW/facet at 50% duty cycle.

affects the antiguiding loss α_R [equation(4)]. Thus, it is not surprising that the lateral far-field pattern changes shape and that the peak of the main lobe drifts slightly to one side. By contrast, in symmetric leaky structures (ref. 14) (i.e., constricted double-heterojunction lasers with large optical cavity, CDH-LOC) the position of the main lobe is stable with drive. Furthermore, CDH-LOC devices have demonstrated single-mode operation to much higher output powers: 40 mW/facet cw and 100 mW/facet at 50% duty cycle (ref. 65). Thus, while initially thin-active-layer semileaky devices were used for optical recording (ref. 63), currently we use CDH-LOC devices (ref. 66).

VI. CONCLUSION

In this report we present a class of mode-stabilized devices that are quite versatile and relatively easy to fabricate: one-step liquid-phase epitaxy over channeled substrates followed by standard oxide-stripe contact formation. Lateral mode control is achieved by active-layer-thickness variations above the mesa between two channels. Current flow uniformity across the lasing cavity is assured by the device geometry (i.e., the lasing cavity is on the least resistive path between the contact and the highly conductive substrate). Thus, as opposed to all other types of channeled substrate devices, CDH lasers do not require tight current confinement in order to achieve fundamental mode lasing. The current that is not used in lasing gives on one hand a less efficient device (i.e., higher thresholds and lower external differential quantum efficiencies), but on the other hand it provides remarkable device stability with respect to changes in ambient temperature.

To summarize, for ridge-guide devices we obtain: single-mode (spatial and frequency) cw operation to 7 mW/facet; threshold currents as low as 28 mA; second-harmonic distortion between -57 and -40 dB below the fundamental level; temperature coefficients T_o as high as 375 and 310°C in pulsed and cw operation, respectively; virtually constant external differential quantum efficiencies to 100°C; cw and pulsed operation to record-high ambient temperatures: 170 and 280°C, respectively. Semileaky CDH lasers have mode-dependent radiation losses which allow single-mode (spatial and frequency) cw operation to 20 mW/facet in lasing spots as wide as 7 μm and single-lobe operation at 50% duty cycle to 50 mW/facet. We show in Table 1 a comparison between various CDH devices, including the high-power CDH-LOC laser (ref. 14).

Both ridge-guide and semileaky-guide devices have been lifetested. In preliminary tests we have found that devices with residual channels on the top surface and bonded with indium can have high thermal resistance values: 100 to 200°C/W and consequently poor life at elevated temperatures. This problem appears to be related to the peculiarities of In solder. When the CDH structures were grown such that the top surface is virtually flat (fig. 12), then thermal resistance values as low as 20°C/W were obtained for 250-μm-long devices. Devices of low thermal resistance gave, as expected, best reliability when tested at 70°C. We have many devices which have passed the 5000-hour mark

TABLE 1. CONSTRICTED DOUBLE-HETEROJUNCTION DIODE LASERS

Structure	Type	Single-Mode cw Output Power (mW)	Typical Spot Size (μm)	T_o (°C)
Three-Layer DH	Ridge guide	3-7	2.5x0.6	240-375
	Semileaky guide	10-15	4.0x0.6	140-170
Large Optical Cavity	Leaky cavity	40-50	6.0x1.5	70-100

at 70°C and the 15,000-hour mark at room temperature, and one device has continuously operated at 70°C for 18,830 hours.

Constricted double-heterojunction diode lasers have demonstrated outstanding cw and pulsed electro-optical characteristics, which make them promising for use in optical communication applications including those cases where single-mode characteristics are desired, such as wavelength multiplexing.

REFERENCES

1. D. Botez: Single-Mode AlGaAs Diode Lasers. J. Opt. Comm., vol. 1, no. 2, 1980, pp. 42-50. Also D. Botez and G. Herskowitz: Components for Optical Communications Systems: A Review. Proc. IEEE, vol. 68, June 1980, pp. 689-732.
2. M. Nakamura: Single Mode Operation of Semiconductor Injection Lasers. IEEE Trans. Circuits and Systems, vol. CAS-26, no. 12, 1979, pp. 1055-1065.
3. S. Wang, C.-Y. Chen, A. S.-H. Liao, and L. Figueroa: Control of Mode Behavior in Semiconductor Lasers, IEEE J. Quantum Electron., vol. QE-17, no. 4, 1981, pp. 453-469.
4. R. D. Burnham and D. R. Scifres: Etched Buried Heterostructure GaAs/GaAlAs Injection Lasers. Appl. Phys. Lett., vol. 27, no. 10, 1975, pp. 510-511.
5. D. Botez, W. Tsang, and S. Wang: Growth Characteristics of GaAs-$Ga_{1-x}Al_xAs$ Structures Fabricated by Liquid-Phase Epitaxy Over Preferentially Etched Channels. Appl. Phys. Lett., vol. 28, no. 4, 1976, pp. 234-237.
6. P. A. Kirkby and G. H. B. Thompson: Channeled Substrate Buried Heterostructure GaAs-(GaAl)As Injection Lasers. J. Appl. Phys., vol. 47, no. 10, 1976, pp. 4578-4589.
7. L. Figueroa and S. Wang: Inverted-Ridge-Waveguide Double-Heterostructure Injection Laser with Current and Lateral Optical Confinement. Appl. Phys. Lett., vol. 31, July 1977, pp. 45-47.
8. K. Aiki, M. Nakamura, T. Kuroda, J. Umeda, R. Ito, N. Chinone, and M. Maeda: Transverse Mode Stabilized Al_xGa_{1-x} Injection Lasers with Channel-Substrate-Planar Structures. IEEE J. Quantum Electron., vol. QE-14, no. 2, 1978, pp. 89-97.
9. D. Botez and P. Zory: Constricted Double-Heterostructure (AlGa)As Diode Lasers. Appl. Phys. Lett., vol. 32, no. 4, 1978, pp. 261-263.
10. D. Botez: Single-Mode CW Operation of 'Double-Dovetail' Constricted DH (AlGa)As Diode Lasers. Appl. Phys. Lett., vol. 33, no. 10, 1978, pp. 872-874.

11. T. Sugino, K. Itoh, M. Wada, H. Shimizu, and I. Teramoto: Fundamental Transverse and Longitudinal Mode Oscillation in Terraced Substrate GaAs-(GaAl)As Lasers. IEEE J. Quantum Electron., vol. QE-15, no. 8, 1979, pp. 714-726.

12. T. Furuse, I. Sakuma, Y. Ide, K. Nishida, and F. Saito: Transverse Mode Stabilized AlGaAs DH Laser Having a Built-In Plano-Convex Waveguide. Fifth European Conference on Opt. Communications, Paper 2.2, Amsterdam, September 1979.

13. R. D. Burnham, D. R. Scifres, W. Streifer, and S. Peled: Nonplanar Large Optical Cavity GaAs/GaAlAs Semiconductor Laser. Appl. Phys. Lett., vol. 35, no. 10, 1979, pp. 734-737.

14. D. Botez: CW High-Power Single-Mode Operation of Constricted Double-Heterojunction AlGaAs Lasers with a Large Optical Cavity, Appl. Phys. Lett., vol. 36, no. 3, 1980, pp. 190-192.

15. E. Oomura, H. Higuchi, R. Hirano, H. Namizaki, T. Murotani, and W. Susaki: Transverse Mode Control in InGaAsP/InP Buried Crescent Diode Lasers. Electron. Lett., vol. 17, January 1981, pp. 83-84.

16. K. Kishino, Y. Suematsu, Y. Takahashi, T. Tanbunek, and Y. Itaya: Fabrication and Lasing Properties of Mesa Substrate Buried-Heterostructure GaInAsP/InP Lasers at 1.3 μm Wavelength. IEEE J. Quantum Electron., vol. QE-16, no. 2, 1980 pp. 160-165.

17. J. J. Coleman and P. D. Dapkus: Single-Longitudinal-Mode Metalorganic Chemical-Vapor-Deposition Self-Aligned GaAlAs-GaAs Double-Heterostructure Lasers. Appl. Phys. Lett., vol. 37, no. 3, 1980, pp. 262-264.

18. D. Botez and J. C. Connolly: Low-Threshold High-T_o Constricted Double Heterojunction AlGaAs Diode Lasers. Electron. Lett., vol. 16, no. 25, 1980, pp. 942-944.

19. K. Funakoshi, A Doi, K. Aiki, and R. Ito: Liquid Phase Epitaxial Growth of $Ga_{1-x}Al_xAs$ on Channeled Substrates. J. Cryst. Growth, vol. 45, 1978, pp. 252-257.

20. V. M. Andreev, V. V. Egorov, A. V. Syrbu, V. G. Trofim, and V. P. Yakovlev: Liquid-Phase Epitaxy of AlGaAs Heterostructures on Profiled Substrates. J. Cryst. Res. Tech., vol. 15, no. 4, 1980, pp. 379-385.

21. P. A. Kirkby: Channelled-Substrate Narrow-Stripe GaAs/GaAlAs Injection Laser with Extremely Low Threshold Currents. Electron. Lett., vol. 15, no. 25, 1979, pp. 824-825.

22. M. Ayabe, O. Matsuda, M. Dosen, S. Santa, and N. Watanabe: An Improved Etched Buried Heterostructure Laser with Reduced Threshold Current. Japan. J. Appl. Phys., vol. 19, Supplement 19-1, 1980, pp. 399-402.
23. D. Botez, J. C. Connolly, D. B. Gilbert, and M. Ettenberg: Very Low Threshold-Current Temperature Sensitivity in Constricted Double--Heterojunction AlGaAs Lasers. J. Appl. Phys., vol. 52, no. 6, 1981, pp. 3840-3844.
24. T. Sugino, H. Shimizu, M. Wada, and K. Itoh: Fundamental Tranverse Mode Oscillation Terraced Substrate Semiconductor Lasers. Natl. Tech. Rep. (Japan), vol. 25, December 1979, pp. 1110-1121 (in Japanese).
25. D. Botez: Planar and Inverted-Ridge GaAs Waveguide Lasers: Device Characteristics and Studies of Liquid-Phase Epitaxy Growth. PhD Thesis, U. of California, Berkeley, December, 1976.
26. C. P. Lee, I. Samid, A. Gover, and A Yariv: Low-Threshold Room-Temperature Embedded Heterostructure Lasers. Appl. Phys. Lett., vol. 29, no. 6, 1976, pp. 365-367.
27. J. W. Cahn and D. W. Hoffman: A Vector Thermodynamics for Anisotropic Surfaces - II Curved and Faceted Surfaces. Acta Metallurgica, vol. 22, October 1974, pp. 1205-1214.
28. H. Kogelnik: An Introduction to Integrated Optics. IEEE Trans. Microwave Theory Tech., vol. MTT-23, January 1975, p. 1.
29. W. Streifer and E. Kapon: Application of the Equivalent-Index Method to DH Diode Lasers. Appl. Opt., vol. 18, November 1979, pp. 3724-3725.
30. J. Buus: A Model for the Static Properties of DH Lasers. Opt. & Quantum Electron., vol. 10, 1978, pp. 459-474.
31. H. Kressel and J. K. Butler: Semiconductor Lasers and Heterojunction LED's. Academic Press, 1977.
32. D. Botez: Analytical Approximation of the Radiation Confinement Factor for the TE_o Mode of a Double Heterojunction Laser. IEEE J. Quantum Electron., vol. QE-14, April 1978, pp. 230-232.
33. D. Botez: InGaAsP/InP Double-Heterojunction Lasers: Simple Expressions for Wave Confinement, Beamwidth, and Threshold Current Over Wide Ranges in Wavelength (1.1-1.65 μm). IEEE J. Quantum Electron., vol. QE-17, no. 2, 1981, pp. 178-186.

34. K. Moriki, K. Wakao, M. Kitamura, K. Iga, and Y. Suematsu: Single Transverse Mode Operation of Terraced Substrate GaInAsP/InP Lasers at 1.3 μm Wavelength. Japan. J. Appl. Phys., vol. 19, no. 11, 1980, pp. 2191-2196.
35. D. B. Hall and C. Yeh: Leaky Waves in a Heteroepitaxial Film. J. Appl. Phys., vol. 44, no. 5, 1973, pp. 2271-2274.
36. R. W. H. Engelmann and D. Kerps: Leaky Modes in Active Three-Layer Slab Waveguides. IEEE Proc., vol. 127, no. 6, 1980, pp. 330-336.
37. T. Kuroda, M. Nakamura, K. Aiki, and J. Umeda: Channelled-Substrate-Planar Structure $Al_xGa_{1-x}Sa$ Lasers: An Analytical Waveguide Study. Appl. Optics, vol. 17, October 1978, pp. 3264-3267.
38. H. Ishikawa, K. Hanamitsu, N. Takagi, T. Fujiwara, and M. Takusagawa: Separated Multiclad-Layer Stripe-Geometry GaAsAs DH Laser. IEEE J. Quantum Electron., vol. QE-17, no. 7, 1981, pp. 1226-1234.
39. P. A. Kirkby, J. Curtis, R. S. Baulcomb, R. G. Plumb, J. E. A. Whiteaway, and A. R. Goodwin: Waveguide Control in GaAs/GaAlAs Channelled Substrate Narrow Stripe Lasers. 7th IEEE Internatl Semicon. Laser Conf., Paper P2, Brighton, England, September 1980.
40. L. Figueroa: Double-Heterostructure Injection Lasers with Lateral Mode Control. PhD Thesis, U. of California, Berkeley, December 1978.
41. T. Tsukada, K. Saito, N. Shige, and Y. Shima: Reduction of Threshold Current of Buried-Heterostructure Injection Lasers. Proc. 7th Conf. on Solid State Devices, Tokyo 1975, Japan. J. Appl. Phys., Supplement vol. 15, 1976, pp. 289-292.
42. W. T. Tsang, R. A. Logan, and M. Ilegems: High-Power Fundamental Transverse-Mode Stripe Buried Heterostructure Lasers with Linear Light-Current Characteristics. Appl. Phys. Lett., vol. 32, March 1978, pp. 311-314.
43. R. L. Hartman, R. A. Logan, L. A. Koszi, and W. T. Tsang: The cw Electro-optical Properties of (AlGa)As Modified-Strip Buried-Heterostructure Lasers. J. Appl. Phys., vol. 51, no. 4, 1980, pp. 1909-1918.
44. H. F. Lockwood and M. Ettenberg: Thin Solution Multiple Layer Epitaxy. J. Cryst. Growth, vol. 15, 1972, pp. 81-83.
45. M. Ettenberg and H. F. Lockwood: Low-Threshold-Current cw Injection Lasers. Fiber & Int. Opt., vol. 2, 1969, pp. 47-61.
46. D. Botez: Near and Far-Field Analytical Approximations for the Fundamental Mode in Symmetric Waveguide DH Lasers. RCA Rev., vol. 39, no. 4, 1978, pp. 577-603.

47. I. Ladany, H. J. Wolkstein, D. Botez, R. S. Crandall, B. R. Dornan, D. R. Patterson, and B. E. Tompkins: A 500 MHz Driver for Single-Mode Fiber-Optic Communication Systems. Tech. Digest of Int. Elec. Dev. Mtg., Paper 25-2, pp. 630-633, Washington, DC, December 1978.
48. W. Streifer, R. D. Burnham, and D. R. Scifres: Channelled Substrate Nonplanar Laser Analysis - Part I: Formulation and Plano-Convex Waveguide Laser. IEEE J. Quantum Electron., vol. QE-17, no. 5, 1981, pp. 736-745.
49. F. Stern: Gain-Current Relation for GaAs Lasers with n-Type and Undoped Active Layers. IEEE J. Quantum Electron., vol. QE-9, February 1973, pp. 290-294.
50. D. Botez, J. C. Connolly, and D. B. Gilbert: High-Temperature cw and Pulsed Operation in Constricted Double-Heterojunction AlGaAs Diode Lasers. Appl. Phys. Lett., vol. 39, no. 1, 1981, pp. 3-6.
51. J. R. Pawlik, W. T. Tsang, F. R. Nash, R. L. Hartman, and V. Swaminathan: Reduced Temperature Dependence of Threshold of (Al,Ga)As Lasers Grown by Molecular Beam Epitaxy. Appl. Phys. Lett., vol. 38, no. 12, 1981, pp. 974-977.
52. H. S. Sommers: Experimental Properties of Injection Laser: VIII Narrow Stripe Lasers with Rigid Waveguide. J. Appl. Phys., vol 50, no. 11, 1979, pp. 6621-6629.
53. M. Ettenberg: A New Dielectric Facet Reflector for Semiconductor Lasers Appl. Phys. Lett., vol. 32, 1976, pp. 724-725.
54. T. Kobayashi and Y. Furukawa: Temperature Distributions in the GaAs-AlGaAs Double-Heterostructure Laser Below and Above the Threshold Current. Japan. J. Appl. Phys., vol. 14, no. 12, 1975, pp. 1981-1986.
55. D. H. Newman, D. J. Bond, J. Stefani: Thermal-Resistance Models for Proton-Isolated Double-Heterostructure Lasers. IEEE Solid-State and Electron Devices, vol. 2, no. 2, 1978, pp. 41-46.
56. E. Duda, J.-C. Carballes, and J. Appruzzese: Thermal Resistance and Temperature Distribution in Double-Heterostructure Lasers: Calculations and Experimental Results. IEEE J. Quantum Electron., vol. QE-15, no. 8, 1979, pp. 812-817.
57. N. K. Dutta and R. J. Nelson: Temperature Dependence of Threshold in InGaAsP/InP DH Lasers and Auger Recombination. Appl. Phys. Lett., vol. 38, March 1981, pp. 407-409.

58. K. Saito and R. Ito: Buried Heterostructure AlGaAs Lasers. IEEE J. Quantum Electron., vol. QE-16, no. 2, 1980, pp. 205-215.
59. L. Figueroa: Study of Mode-Locking in (GaAl)As Injection Lasers. IEEE J. Quantum Electron., vol. QE-17, no. 6, 1981, pp. 1074-1085.
60. T. Ikegami: Spectrum Broadening and Tailing Effect in Direct-Modulated Injection Lasers. Proc. 1st European Conf. Optical Fibre Commun., London, England, 1975, p.111.
61. N. Chinone, K. Aiki, M. Nakamura, and R. Ito: Effects of Lateral Mode and Carrier Density Profile on Dynamic Behaviors of Semiconductor Lasers. IEEE J. Quantum Electron., vol. QE-14, no. 8, 1978, pp. 625-631.
62. D. R. Scifres, W. Streifer, and R. D. Burnham: Leaky Wave Room-Temperature Double Heterostructure GaAs: GaAlAs Diode Laser. Appl. Phys. Lett., vol. 29, no. 1, 1976, pp. 23-25.
63. D. Botez, F. W. Spong, and M. Ettenberg: High Power Constricted Double-Heterojunction AlGaAs Lasers for Optical Recording. Appl. Phys. Lett., vol. 36, no. 1, 1980, pp. 4-6.
64. W. Streifer, R. D. Burnham, and D. R. Scifres: Symmetrical and Asymmetrical Waveguiding in Very Narrow Conducting Stripe Lasers. IEEE J. Quantum Electron., vol. QE-15, no. 3, 1979, pp. 136-141.
65. D. Botez and J. C. Connolly: Single-Mode Positive Index Guided cw CDH-LOC AlGaAs Lasers with Low Threshold-Current Temperature Sensitivity. Appl. Phys. Lett., vol. 38, no. 9, 1981, pp. 658-660.
66. R. A. Bartolini, A. E. Bell, and F. W. Spong: Diode Laser Optical Recording Using Trilayer Structures. IEEE J. Quantum Electron., vol. QE-17, no. 1, 1981, pp. 69-77.

1. Report No.	2. Government Accession No.	3. Recipient's Catalog No.
NASA CR-3520		

4. Title and Subtitle	5. Report Date
STUDIES OF SINGLE-MODE INJECTION LASERS AND OF QUATERNARY MATERIALS. VOLUME I – SINGLE-MODE CONSTRICTED DOUBLE-HETEROJUNCTION AlGaAs DIODE LASERS	April 1982
	6. Performing Organization Code

7. Author(s)	8. Performing Organization Report No.
Dan Botez	PRRL-81-CR-29 (I)
	10. Work Unit No.

9. Performing Organization Name and Address	11. Contract or Grant No.
RCA Laboratories Princeton, NJ 08540	NAS1-15440
	13. Type of Report and Period Covered Contractor Report 2-4-80 to 5-15-81

12. Sponsoring Agency Name and Address	14. Sponsoring Agency Code
National Aeronautics and Space Administration Washington, DC 20546	

15. Supplementary Notes

16. Abstract

Constricted double-heterojunction (CDH) lasers are presented as the class of single-mode nonplanar-substrate devices for which the lasing cavity is on the least resistive electrical path between the contact and the substrate. Various types of CDH structures are discussed while treating three general topics: liquid-phase epitaxy over channeled substrates, lateral mode control, and current control in nonplanar-substrate devices. "Ridge-guide" CDH lasers have positive-index lateral-mode confinement and provide: single-mode cw operation to 7 mW/facet at room temperature and to 3 mW/facet at 150°C; light-current characteristics with second-harmonic distortion as low as -57 dB below the fundamental level; threshold-current temperature coefficients, T_o, as high as 375°C (pulsed) and 310°C (cw); constant external differential quantum efficiency to 100°C; and lasing operation to 170°C cw and 280°C pulsed. "Semileaky-guide" CDH lasers have an asymmetric leaky cavity for lateral-mode confinement and provide single-mode operation to 15 to 20 mW/facet cw and to 50 mW/facet at 50% duty cycle. Modulation characteristics and preliminary reliability data are also discussed.

Constricted double-heterojunction diode lasers have demonstrated outstanding cw and pulsed electro-optical characteristics, which make them promising for use in optical communication applications including those cases where single-mode characteristics are desired, such as wavelength multiplexing.

17. Key Words (Suggested by Author(s))	18. Distribution Statement
Single-mode injection lasers Quaternary materials Electro-optic effects InGaAsP junction waveguides Constricted double-heterojunction laser	Unclassified - Unlimited Subject Category 34

19. Security Classif. (of this report)	20. Security Classif. (of this page)	21. No. of Pages	22. Price
Unclassified	Unclassified	69	A04

For sale by the National Technical Information Service, Springfield, Virginia 22161 NASA-Langley, 1982